NATIONAL ENERGY TECHNOLOGY LABORATORY

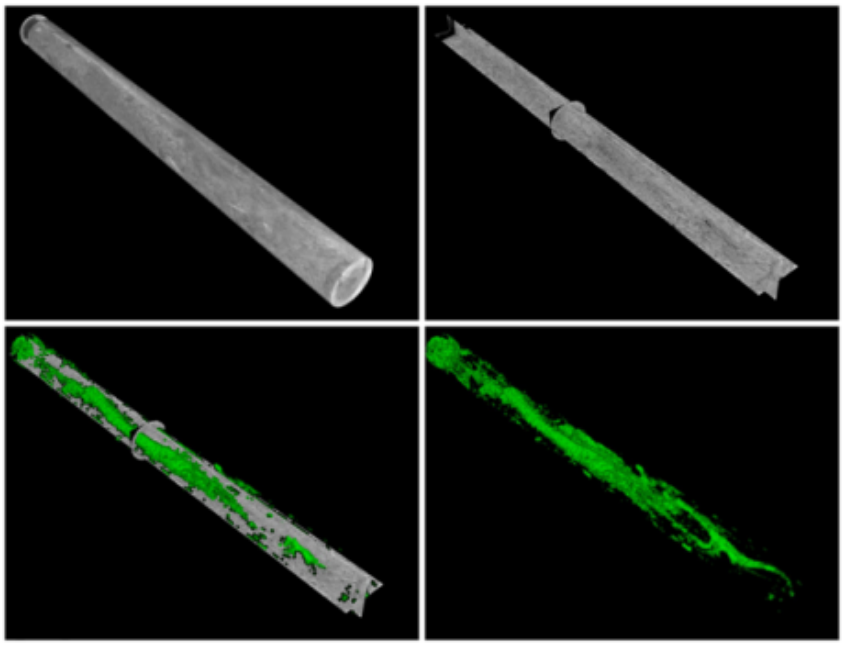

Field-Generated Foamed Cement: Initial Collection, Computed Tomography, and Analysis

20 July 2015

U.S. DEPARTMENT OF ENERGY

Office of Fossil Energy

NETL-TRS-5-2015

Disclaimer

Cover Illustration: Three dimensional (3-D) reconstructions of computed tomography scans of pressurized field foamed cement sample D2. Injection port is in the bottom right of each image; retracting piston in the top left of each image. The top left image is a reconstruction of the entire cement sample. The top right image is an orthoslice along the primary directions of the vessel. The bottom left image is an othroslice and a 3-D rendering of isolated low density zones. The bottom right image is a 3-D rendering of just the low density zones.

Suggested Citation: Kutchko, B.; Crandall, D.; Moore, J.; Gill, M.; McIntyre, D.; Rosenbaum, E.; Haljasmaa, I.; Strazisar, B.; Spaulding, R.; Harbert, W.; Benge, G.; Cunningham, E.; Lawrence, W.; DeBruijn, G.; Gardner, C. *Field-Generated Foamed Cement: Initial Collection, Computed Tomography, and Analysis*; NETL-TRS-5-2015; EPAct Technical Report Series; U.S. Department of Energy, National Energy Technology Laboratory: Morgantown, WV, 2015; p 48.

An electronic version of this report can be found at:

http://www.netl.doe.gov/research/on-site-research/publications/featured-technical-reports

https://edx.netl.doe.gov/offshore

Field-Generated Foamed Cement: Initial Collection, Computed Tomography Scanning, and Analysis

Barbara Kutchko[1], Dustin Crandall[2], Johnathan Moore[2,3], Magdalena Gill[2,3], Dustin McIntyre[2], Eilis Rosenbaum[1], Igor Haljasmaa[1, 3], Brian Strazisar[4], Rick Spaulding[5], William Harbert[5], Glen Benge[6], Gunnar DeBruijn[7], Joe Shine[8], Craig Gardner[9]

[1] U.S. Department of Energy, Office of Research and Development, National Energy Technology Laboratory, 626 Cochrans Mill Road, Pittsburgh, PA 15236

[2] U.S. Department of Energy, Office of Research and Development, National Energy Technology Laboratory, 3610 Collins Ferry Road, Morgantown, WV 26507

[3] U.S. Department of Energy, National Energy Technology Laboratory, URS, 3610 Collins Ferry Road, Morgantown, WV 26507

[4] RJ Lee Group, 350 Hochberg Road, Monroeville, PA 15146

[5] University of Pittsburgh, 4107 O'Hara Street, Pittsburgh, PA 15260

[6] Benge Consulting, 86 East Slatestone Circle, The Woodlands, TX 77382

[7] Schlumberger, 300 Schlumberger Drive, Sugar Land, TX 77478

[8] Baker Hughes, 17021 Aldine Westfield Road, Houston, TX 77073

[9] Chevron, 3901 Briarpark Drive, Houston, TX 77042

NETL-TRS-5-2015

20 July 2015

NETL Contacts:

Barbara Kutchko, Principal Investigator

Kelly Rose, Technical Coordinator

Cynthia Powell, Focus Area Lead

This page intentionally left blank.

Table of Contents

This page intentionally left blank.

List of Figures

List of Tables

Acronyms, Abbreviations, and Symbols

Term	Description
µA	Microampere, 10^{-6} amperes
µm	Micrometer, 10^{-6} meter
2-D	Two-dimensional
3-D	Three-dimensional
API	American Petroleum Institute
BSD	Bubble size distribution
CP	Constant pressure
CT	Computed tomography
CTN	Computed tomography number
DOE	Department of Energy
DOT	Department of Transportation
FCG	Foamed cement generator
HSE	Health, safety, and/or environmental
kV	Kilovolt, 1000 volts
NETL	National Energy Technology Laboratory
NPT	National pipe thread
NSI	North Star Imaging
Re	Reynolds number
RP	Recommended Practice
SEM	Scanning electron microscopy

Acknowledgments

This work was completed as part of National Energy Technology Laboratory (NETL) research for the U.S. Department of Energy's (DOE) Complementary Research Program under Section 999 of the Energy Policy Act of 2005. The authors wish to acknowledge Roy Long (NETL Strategic Center for Natural Gas and Oil) and Elena Melchert (DOE Office of Fossil Energy) for programmatic guidance, direction, and support. In addition, the authors extend a special thanks to Roy Long for technical guidance as well. We would like to thank Bryan Tennant, Karl Jarvis and Roger Lapeer for making the CT scanner lab functional. Thanks to Jim Fazio for superior laboratory assistance. The authors extend a special thanks to Erick Cunningham and Woody Lawrence.

EXECUTIVE SUMMARY

National Energy Technology Laboratory (NETL) researchers have produced the first X-ray computed tomography (CT) three dimensional (3-D) images of field-generated foamed cement across a range of foam qualities and pressures. Foamed cement is widely used for cementing oil and gas wells requiring lightweight slurries, gas migration prevention, or wells with high stress environments. Foamed cement was collected into sampling vessels utilizing the same full scale industrial equipment used to execute wellbore cementing field operations. A unique methodology was developed and implemented to capture the cement under representative field pressure conditions. These samples were then transported to NETL in Morgantown, WV to be analyzed.

CT imaging enabled the assessment and quantification of the foam structure, quality, and void distribution providing the industry a better understanding of foamed cement behavior. The initial field-generated foamed cement testing revealed the structure of the cement was non-uniform, with distinguishable low and high density zones dispersed throughout the sample vessels. The heterogeneous structure suggests the motion of the foamed cement slurry within the vessels influenced the distribution of voids within the final solidified product. The variation observed in these samples was significantly different from distributions observed in laboratory-generated foamed cement samples that have historically been used to quantify foamed cement properties (Kutchko et al., 2013, 2014).

Work is continuing to evaluate in greater detail the field-generated samples using higher resolution CT imaging and analysis. Flow properties of the slurry as well as the mechanical properties of the set cement are being simulated to provide a relationship between the observed structures and wellbore stabilization properties for use in wellbore construction. In addition, laboratory-prepared foamed cement is being generated at representative pressures and being studied under more controlled conditions than the feasibility of multiple iterations using large scale field generation equipment. Together, the research will provide a better understanding of the effects that foamed cement generation, transport downhole, and delivery to the wellbore annulus have on the overall isolation performance. This report is a description of the early results found thus far in this joint NETL and industry study.

1. INTRODUCTION

Foamed cement is created when a gas, typically nitrogen, is stabilized in the form of microscopic bubbles within cement slurries (Harms and Febus, 1985; Nelson, 2006). Foamed cements are low-density cement systems used in formations unable to support the annular hydrostatic pressure of conventional cement slurries (Nelson, 2006; Harlan et al., 2001). The use of foamed cement for its low density is well documented in literature (Benge and Poole, 2005; Harlan et al., 2001; White et al., 2000; Kopp et al., 2000; Frisch et al., 1999; Benge et al., 1996; Thayer et al., 1993; Harms and Febus, 1985). The benefits of using foamed cement include the ability to change the foamed cement density at the rig site by simply changing the quantity of gas without significantly affecting slurry properties and foamed cement does not have the pressure limitations found with ultra-lightweight extenders (Benge and Poole, 2005; Nelson, 2006).

The use of foamed cement has expanded into regions with high-stress environments, for example, in deepwater operations (Nelson, 2006; Rae and Lullo, 2004; White et al., 2000; Judge and Benge, 1998; Benge et al., 1996). Foamed cements, usually lower density systems, can be used when encountering lost circulation or depleted zones, and reduced hydrostatic pressures are required to prevent losses (Frisch et al., 1999; Thayer et al., 1993). To mitigate shallow hazards in deepwater Gulf of Mexico, foamed cement systems are the system of choice (American Petroleum Institute, API RP 65) and are used to prevent compaction damage in deepwater operations (Taiwo and Ogbonna, 2011; Harlan et al., 2001; White et al., 2000; Kopp et al., 2000; Moore et al., 2000; Frisch et al., 1999; API, 2010).

In some cases, foamed cement is used to modify mechanical parameters of the resulting slurry. The entrained gas in the cement creates a network within the matrix of the cement which in turn exhibits a more elastic response—foamed cement has a lower Young's modulus than conventional cement slurries (Iverson et al., 2008; Deeg et al., 1999). This is significant because cement slurries with lower Young's moduli are more resistant to the common mechanical stresses associated with well operations (Kopp et al., 2000; Deeg et al., 2008). As such, foamed cements are often used to prevent stress cracking in the cement sheath due to temperature and pressure cycles which improve long-term zonal isolation (Benge et al., 1996). Foamed cement also exhibits superior fluid displacement and minimal shrinkage (and hence, gas-migration control), therefore, making it a robust and versatile option for wellbore integrity (White et al., 2000).

Foamed cement is generated with temperature and pressure at the surface or well site and is then pumped into wells through high-pressure treating lines. After the final placement of the foamed cement into the wellbore annulus it cures under another set of downhole temperatures and pressures, thus the time rate of change of the fluxes the foamed cement sees during placement can likely affect the final performance if not accounted for. Foamed cement is rarely re-exposed to atmospheric pressure after generation unless circulated back to the surface out of the well; and while quite rare, would be more common for onshore applications. While the foamed cement is in the slurry stage, the nitrogen bubble size and foam stability are greatly affected by temperature, pressure, and shear rate at which the foam is generated. The shear rate is a more commonly a function of the differential pressure applied to the nitrogen side versus the cement side before the comingling of the two phases in the high-pressure treating lines to create a foamed fluid at the surface. Once the cement has cured (hardened), the nitrogen gas bubbles are trapped in place under in situ pressure.

Stable foamed cement has a consistent density along the length of the column with a homogenous distribution of bubbles throughout the same column, commonly known as bubble size distribution (BSD). It has been shown to have a uniform distribution of spherical, discreet bubbles, which ensures that gas will not break out of the slurry (Nelson, 2006; Griffith et al., 2004). Unstable foamed cements may have nonspherical and/or interconnected voids which can result in poorly contained sections caused by channeling in the well and density inhomogeneity (Nelson, 2006; de Rozieres and Ferriere, 1991). These foams develop lower compressive strength and higher permeability than stable foamed cement (Nelson, 2006).

Foamed cements are categorized by the foam quality (Q_{foam}) (Nelson, 2006) which is a measure of the percent of the sample volume with gas voids entrained in the cement; sometimes referred to as the cement matrix. The higher the foam quality, the higher the entrained gas content (e.g. 20% foam quality contains 20% gas by volume). This volume percentage does not include the microscopic pore volume within the cement matrix.

There is a significant knowledge gap regarding the stability and properties of foamed cement as it is placed in the well (Kutchko et al., 2012). Designing foamed cement systems requires understanding the influence of parameters such as temperature, pressure, and shear. The API recommended practice (API, 2004) for generating and testing wellbore foamed cements is done at atmospheric conditions. A comprehensive literature review identified very limited published laboratory studies that examine foamed cement under wellbore conditions (de Rozieres and Ferriere, 1991). de Rozieres & Ferriere (1991) designed a foamed cement generating unit to study foamed systems at a pressure range from 0.1 to 7 MPa (14.5 to 1015 psi). However, the samples needed to be depressurized before analysis. Rapid depressurization of foamed cement samples created at elevated pressure can result in changes to the physical properties of the cement as the nitrogen expands, causing irreversible damage to the bubble structure.

The current study builds on the work presented by de Rozieres and Ferriere (1991) and Kutchko et al. (2013) by using an industrial computed tomography (CT) scanner to obtain foamed cement image data sets in three dimensions (3-D). This report is a first look at ongoing research to assess and quantify the foam structure and quality of foamed cements collected by the same process described above with full scale industrial equipment. Previous work detailed the results of the atmospheric-generated foamed cements (Kutchko et al., 2013, 2014) and set forth a methodology for high resolution image analysis of these samples.

Future reports will detail laboratory-generated foamed cements using the same foamed cement generator (FCG) used in de Rozieres and Ferriere's (1991) previous work, as well as evaluating the mechanical properties. Future work will also be presented on the high resolution CT imaging of these high pressure foamed cement samples to compare and contrast to the atmospherically-generated foamed cement samples. This analysis should help with understanding what laboratory testing conditions may be required to generate acceptable foamed cement systems to be pumped into wellbore environments providing long-term zonal isolation.

For the data presented in this report, the field-generated cement systems were scanned at the same pressure at which they were collected using both a:

1. Low resolution medical CT scanner
2. Higher resolution industrial CT scanner

A correlation will provide a better understanding of the effects that foamed cement production, delivery to the wellbore, annulus, and transport downhole has on the overall isolation process. The results of this research should provide researchers, regulators, and industry knowledge to ensure the safe operation and integrity of wells in which foamed cement systems are used.

2. METHODS

Cement samples were generated using base slurries of API Class H Portland cement (Lafarge, Joppa, IL) with a slurry density of 16.5 lbm/gal (1.97 g/cm^3). The only additives in the system were the foaming agent and a foam stabilizer. The mix water was fresh water from a pond that is on location at the test facility. The pond is fed by a creek that also flows through the location. Samples were collected into 2-in. diameter by 3-ft long cylinders and maintained at elevated operating pressures.

2.1 PRESSURIZED CEMENT SAMPLE VESSELS

Collecting representative samples of foamed cement from the same full scale industrial equipment used to generate foamed cement on location into a well presented a number of challenges. The foam slurry needed to be collected, stored under pressure until it cured, and transported from the job site to NETL's CT scanning facility in Morgantown, WV, USA. After considering several industry devices available for collecting and storing flowing fluids under pressure, the constant pressure (CP) sample cylinder was chosen. The CP sample cylinder is commonly used by refineries to collect fluids flowing under pressure through high pressure pipes while keeping the fluid under constant pressure. The container is a specially designed tube with a pressure gauge on each end. On one side of the tube is an inlet with a ball valve to collect fluid samples. After the inlet, there is a purge valve on the end cap to allow any unwanted fluids or air to be released from the treating line so that a clean sample can be collected in the tube. Inside the tube, the collection fluid retracts a piston. On the other side of the tube is a 0.25 in. inlet so that the tube may be pre-charged with nitrogen gas to a planned pressure. A needle valve connects to the inlet to either trap or slowly release the nitrogen gas. On the outside of the tube is a race with a magnet to track the position of the piston inside the tube. The sample cylinders are U.S. Department of Transportation (DOT) rated and were able to be transported under pressure.

The CP sample cylinders were manufactured in aluminum and stainless steel. The CT scanner has better resolution through the aluminum than through stainless steel; however, the aluminum cylinders are limited to 600 psi working pressure. For this reason, four samples of foamed cement were collected with the aluminum cylinders at 500 psi each, and two samples in stainless steel cylinders at 1,000 psi each. For comparison purposes, the collection schedule included two samples in aluminum cylinders at 20% foam quality, one sample in an aluminum cylinder at 40% foam quality, and one sample in an aluminum cylinder at 30% foam quality. In the stainless steel cylinders one sample at 20% foam quality and one sample at 30% foam quality were collected. All the cylinders were coated to prevent the metal from reacting with the cement slurry. Figure 1 is a photograph of two of the CP sample cylinders.

Figure 1: Photograph of two constant pressure sample cylinders; steel on the left and aluminum on the right.

2.2 PRESSURIZED CEMENT SAMPLE COLLECTION

The design of the experiment for collecting foamed cement samples from 2 in. high-pressure treating lines was an industry first. In order to collect a representative foamed cement sample for CT scanning from industry equipment kits, a method had to be developed. This methodology required sampling a small amount of foamed cement from the high-pressure treating lines while keeping the foamed cement under constant pressure. In addition, the collected foamed cement sample had to cure under the elevated pressure conditions, and was then transported to the lab for analysis. This methodology had to meet the success criteria for no health, safety, and/or environmental (HSE) events that included personal injury as well as equipment damage.

The developed procedure diverted part of the foamed cement downstream of the cement generating equipment from the main treating line into a manifold system that allowed the sampling under pressure while the main treating line remained open to continuous flow. The

diverted treating line described above was called the “sample manifold”. The sample manifold was installed by the addition of “tees”, each connected with a high pressure isolation valve, which would be crossed over (connection which conjoins the outlet to the inlet of different sizes) to the actual sample tube to collect and store the foamed cement samples. The described crossover allowed connection from the 2 in. treating iron to the 0.75 in. national pipe thread (NPT) on the sample cylinder. Figure 2 is an illustration of the sample manifold and diversion/bypass loop.

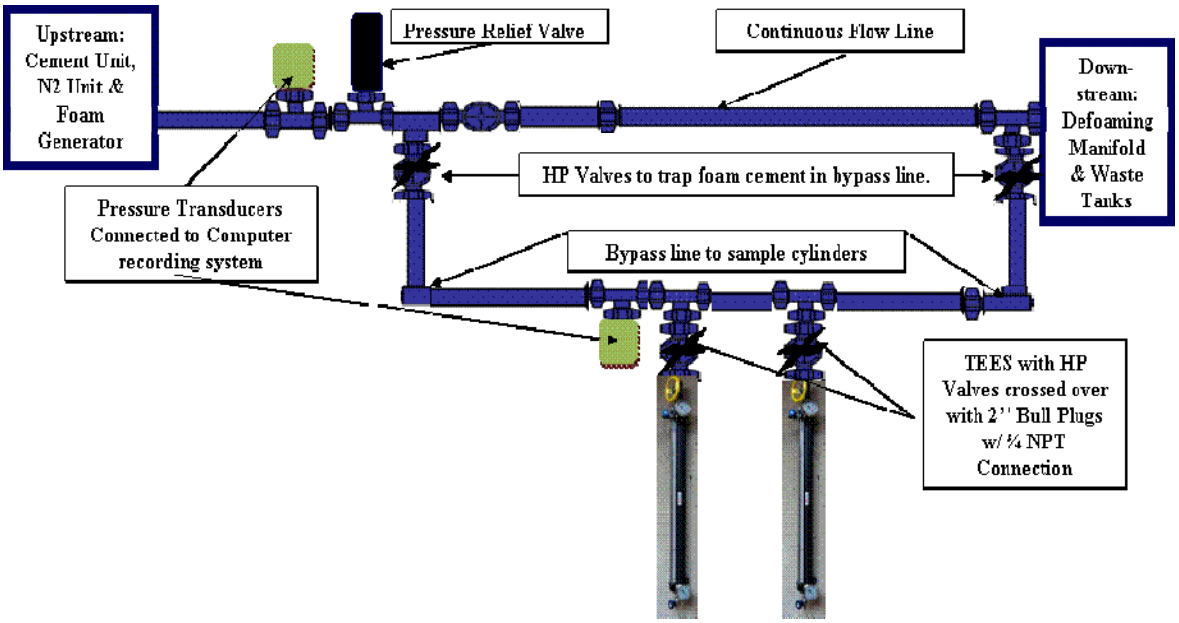

Figure 2: Schematic of the sample manifold for field sample collection.

A pressure relief valve and a digital pressure sensor recorded pressure upstream of the sample manifold for this event. Downstream of the sample manifold, a choke system was installed to maintain enough backpressure on the treating lines to achieve the planned sampling pressures. After the choke system there was an injection point where a defoamer additive was used to break or destabilize the foam cement before being pumped to deceleration disposal tanks.

Enough treating line was connected into the sample manifold bypass loop to create a safe distance from the main treating line. Another digital pressure gauge was attached to the manifold to allow recording of pressure at the sample collection point.

The previously referenced crossover was a 2 in. hammer union consisting of a 2 in. bull plug with a hole drilled through the center and 0.75 in. NPT thread machined into the hole (shown in Figure 3). This bull plug connected to each high-pressure isolation valve on each tee in the sample manifold. The manufactured sample tubes contained 0.75 in. NPT connections so each sample tube connected directly to the bull plug.

Figure 3: Photograph of the crossover between the manifold line and the collection vessel.

Below is the procedure that was used to collect a foamed cement sample with the CP sample cylinder through the sample manifold:

- Open the isolation valves to the sample manifold and the main treating line
- Close the isolation valves below the CP sample cylinders
- Open the ball valve on the CP sample cylinder and close the purge valve on the same cylinder
- Pre-charge the CP sample cylinder with slightly higher than anticipated sampling pressure
- Note: This pressure can be monitored on the pre-charge gauge while the inlet gauge should read 0 psi
- Pump foamed cement slurry through the main line and sample manifold line
- Note: Make the adjustments until the pressure and foam quality are at the planned operating conditions
- Close the isolation valves
- Open one of the high-pressure valves below one of the CP sample cylinders
- Note: The pressure gauge on the inlet side of the CP sample cylinder should show the same pressure as the digital gauge on the sample manifold line
- Open the purge valve until clean foamed cement slurry discharges through the purge valve
- Close the purge valve

- Crack open the pre-charge needle valve to release enough nitrogen gas (N_2) from the pre-charge side so that the piston retracts
- Monitor the piston position and speed by watching the magnet moving through the external sight glass
- Note: The pressure gauges on both sides of the CP sample cylinder should be the same
- When the piston has moved back sufficiently, close the pre-charge needle valve and the piston should stop moving
- Close the inlet ball valve and disconnect the CP sample cylinder from the bull plug
- Note: A sample of foamed cement has now been collected and trapped under pressure in the CP sample cylinder
- Place the CP sample cylinder in a safe place while the foamed cement cures
- Monitor and record the pressure on the CP sample cylinder for 48 hours

Five samples were collected in the first trial (the duplicate 20% quality sample collection in an aluminum CP vessel was unsuccessful due to a rupture disk failure). The recorded parameters for the samples are detailed in Table 1. The foam quality from the sensors during foam generation was calculated from the slurry rate, nitrogen rate, pressure, and temperature in the treating line at the time of the foam generation. The calculated sample cement foam quality was determined from the targeted foam quality and the pressure drop that occurred when taking the sample.

The methodology used to collect field samples made it difficult to obtain any foamed cement below a 30% quality. Obtaining low quality foam samples with this set up was difficult due to the low pressure restriction and the small volume of the lines. The collection at relatively low sample pressures required keeping the pressure low in the treating lines. Pressures in surface lines during normal field operations are typically at 1,000 to 3,000 psi. This methodology operated at lower pressures and rates, and required using the minimum operating pump rate limits for the N_2 pump. Operating the treating lines at 1,000 psi enabled the sample collection to be closer to the foam quality sampling goal. However, operating the treating lines at 500 psi required lower N_2 rates, and of course, half the pressure. The other difficulty is in trapping a small volume of slurry and having to take into account the foam expansion.

There are several relationships or equations used to determine the calculated foam quality which could vary in accuracy. The more accepted relationships to determine foamed cement qualities have been well documented (Nelson et al., 2006). All of the numbers appeared reasonably accurate to the operators performing the sample collection. The foam quality calculated from the sensors while pumping took into account all of the factors (pressure, temperature, flow rates of liquid and N_2). Once pumping was stopped the static pressure gages are the best for indicating what pressure actually went into the cylinder. Hence, the foam quality calculated from pressure was considered reasonable.

These samples were stored near vertical and shipped to the CT scanner facility NETL in Morgantown, WV for analysis.

Table 1: Foamed Cement Sample Parameters

Sample Designation:	A1	A2	E1	D1	D2
Order Collected	**1**	**2**	**3**	**4**	**5**
Targeted Experimental Values					
Sample Quality (%)	30		20	30	
Slurry Rate (bpm)	3		3	3	
N_2 Rate (scf/min)	440		103	195	
Measured Foam Quality (from sensors)	25		16	25	
Sample Line Pressure					
End of Pumping (psi)	1180		790	770	
Before Sample (psi)	1180	940	480	490	387
After Sampling (psi)	940	780	323	387	316
Third Day (psi)	850	650	290	310	290
Calculated Sample Cement Foam Quality					
Q (% from Pressure)	30.1	34.4	33.6	41.2	47.8

2.3 COMPUTED TOMOGRAPHY SCANNING

In X-ray CT scans, grayscale values of the final image are based on the amount of attenuation produced as the X-ray travels through matter. The degree of attenuation that occurs in a given material is defined as the absorption coefficient, which is largely controlled by the density and the effective atomic number of the material. In practice, absolute grayscale values can be further influenced by a range of environmental variables, and often vary from scan to scan. Experimental factors such as room temperature and how long the CT scanner has been running can influence the results. An additional factor is the energy of the penetrating X-rays, because absorption coefficients vary strongly with peak X-ray energy. Post-scan image processing and segmentation, where choice and application of appropriate thresholds is of paramount importance, requires scientific rigor to achieve consistent, repeatable, and statistically significant results (Kutchko et al., 2013).

All the foamed cement samples were scanned in a North Star Imaging (NSI) M-5000 industrial CT scanner at resolutions ranging from 22–41 μm. Field-generated cement samples were also initially scanned using a medical CT scanner (Toshiba Aquilon RXL) to evaluate bulk properties of the cement. The medical CT scanner has a lower resolution than the industrial CT scanner with the ability to generate images with a resolution of 0.43 mm in the scanning plane (X-Y directions) and 0.5 mm along the axial plane (Z direction). However, this scanner is much faster than the industrial CT scanner, can scan large objects all at once, and is useful for bulk characterizations. Small individual bubbles are not visible with the medical CT scanner, but larger air voids and overall structure of the cement can be identified.

All of the aluminum sample containers were scanned with a voltage of 135 kV, a current of 200 mA, an exposure time of 100 ms, and a slice thickness of 0.5 mm. The voxel resolution in the X-

Y plane was set to 0.43 mm. The steel sample container was scanned with an increased exposure time of 500 ms, in an attempt to better penetrate the steel walls of the vessel. Image processing of the medical CT scans was performed with ImageJ (Rasband, 2012). DICOM image files from the Toshiba Aquilion RXL control computer were read into ImageJ as a stack of XY slices for each study. Slices were aligned prior to analysis using the StackReg plugin (Thévenaz et al., 1998).

All foamed cement samples were then scanned in the industrial CT scanner, with a voxel resolution of $(\sim 35\ \mu m)^3$ with scan parameters of 185 kV, a current of 400 μA, and an exposure time of 500 ms. High-resolution industrial CT scans enable researchers to perform more detailed analysis of the structure of this pressurized foamed cement.

3. OBSERVATIONS

The samples were scanned using the CT scanner equipment at NETL in Morgantown WV. Following the CT scanning within the CP vessels, the samples were left to slowly depressurize over the course of several months. This was evident with a slow decline in pressure from gradual escape of gas through the cemented shut valves to atmospheric conditions. No obvious change in the cement structure was observed during this slow depressurization. Several of the CP vessels maintained an elevated pressure. These were depressurized by connecting the CP vessels to an Isco Pump (Teledyne Isco, Lincoln NE) set to maintain a constant flow rate from the vessels of 0.02 ml/min, slowly reducing the pressure within the vessels over several days. Analysis of the depressurized samples will be reported in future reports and is beyond the scope of these initial findings.

3.1 SAMPLE A1

The steel casing of the A1 pressure vessel makes identification of relevant information from these medical CT scans difficult. The high X-ray attenuation of the steel, coupled with the six steel rods around the outside of the pressure vessel created a large amount of noise and distortion of the CT scans. This is most apparent in the middle image of the XZ montages shown in Figure 4. All medical CT scans along the XZ planes, are oriented such that the cement injection ports are at the bottom of the images and the retracting piston within the CP sample cylinders are at the top of the image. Despite the poor image quality of the A1 scans several properties of the foamed cement can be noted. There is a ≈3.8 cm (1.5 in.) region at the top of the vessel, below the CP vessel piston, where the foamed cement is not present. This “gas cap” was evident in the majority of the samples—likely a consequence of the high foam quality captured in the sample collection. Several large bubbles and regions of high and low density are visible through the noise of the scans as well, as is shown in Figure 5. Quantifying these values given the noise of the CT scans is not possible, however. Industrial CT images obtained through the steel were of poor quality as well; none of those results are shown in this document.

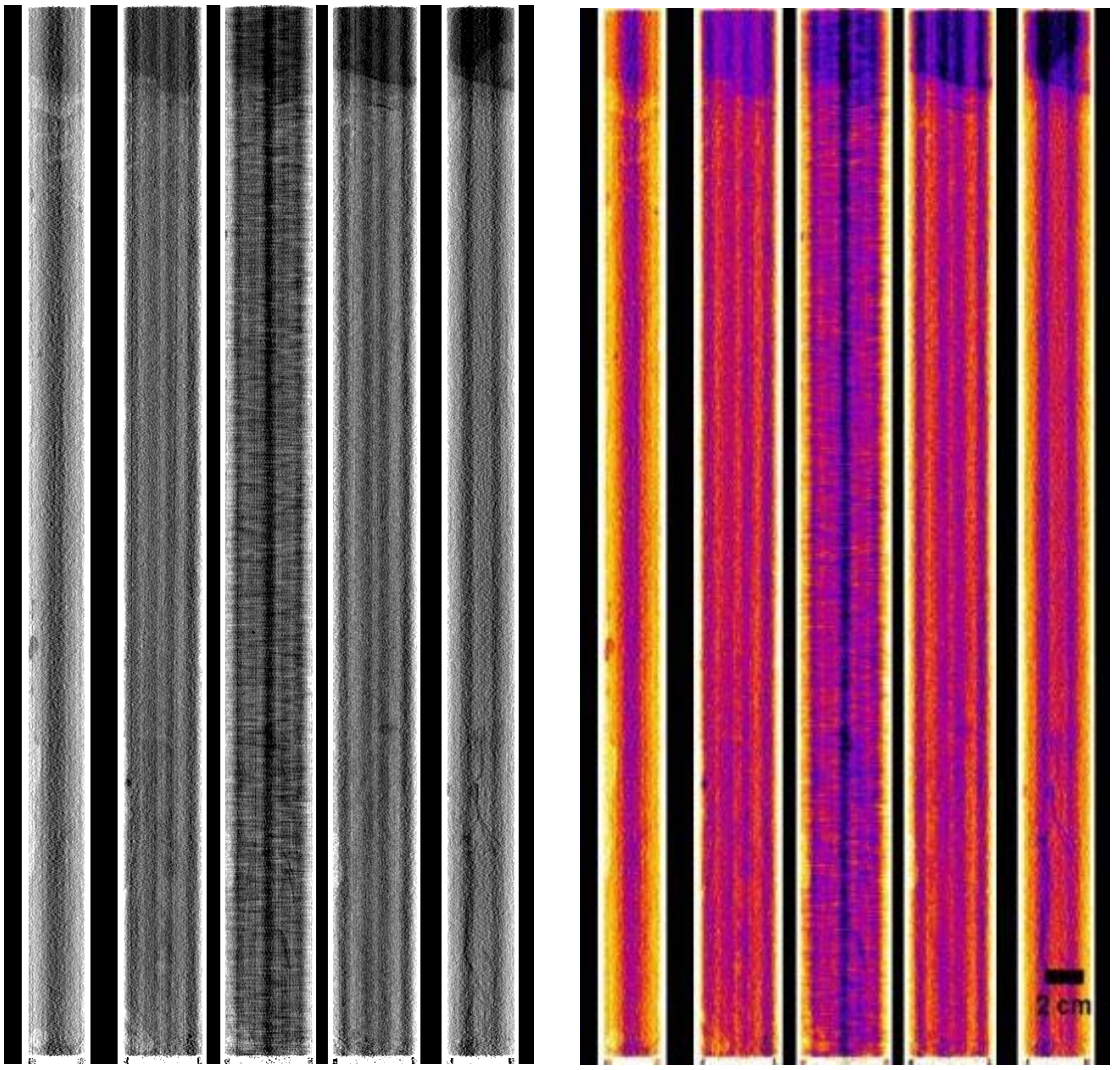

Figure 4: Reconstructed medical CT images of steel vessel A1. Each image is a montage of five cross-sections along the XZ plane of the vessel. Left: a grayscale rendering. Right: a false coloring scheme has been applied. Estimated foam quality 30.5% (Table 1).

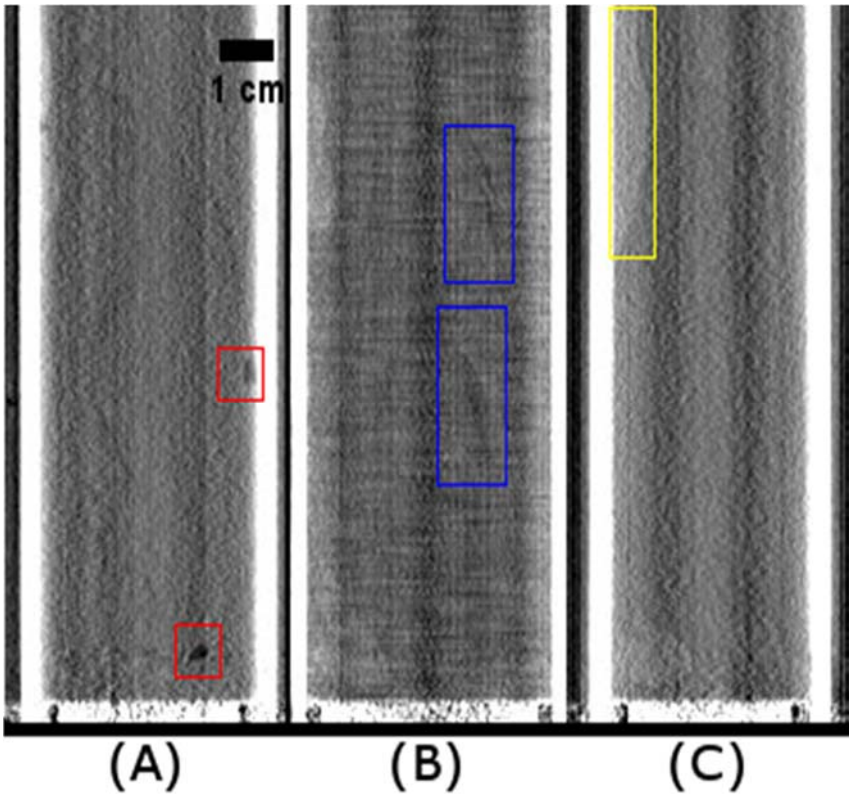

Figure 5: Segment of the reconstructed medical CT images of steel vessel A1. Each image is a cross-section of the bottom 13 cm (5.1 in.) of the vessel. (A) Larger air voids in cement. (B) Elongated low porosity zones in the cement. (C) High density region of the cement.

3.2 SAMPLE D1

The aluminum CP sample vessels were scanned, and more information on the bulk properties and structures was obtained. As shown in Figure 6, the medical CT scanner is able to capture the complexity of the cement structure within the D1 aluminum pressure vessels. In all grayscale CT images shown in this document the darker zones are lower density areas with smaller CT numbers (CTN) and brighter zones are higher density areas with larger CTN. The variation in density throughout the D1 sample is apparent, with zones of high porosity (low density) throughout the vessel. The bubbles clustering are reminiscent of particle clustering in turbulent flows studies in Nasr et al. (2009), due to the vorticity in the flow. An analysis for this study determined that the flow inside the pressure vessel is most likely laminar and is presented in Section 4. Studies are ongoing to determine the effects of vorticity and shear rate on the bubbles. The heterogeneous nature of the foamed cement is readily apparent in these full vessel scans.

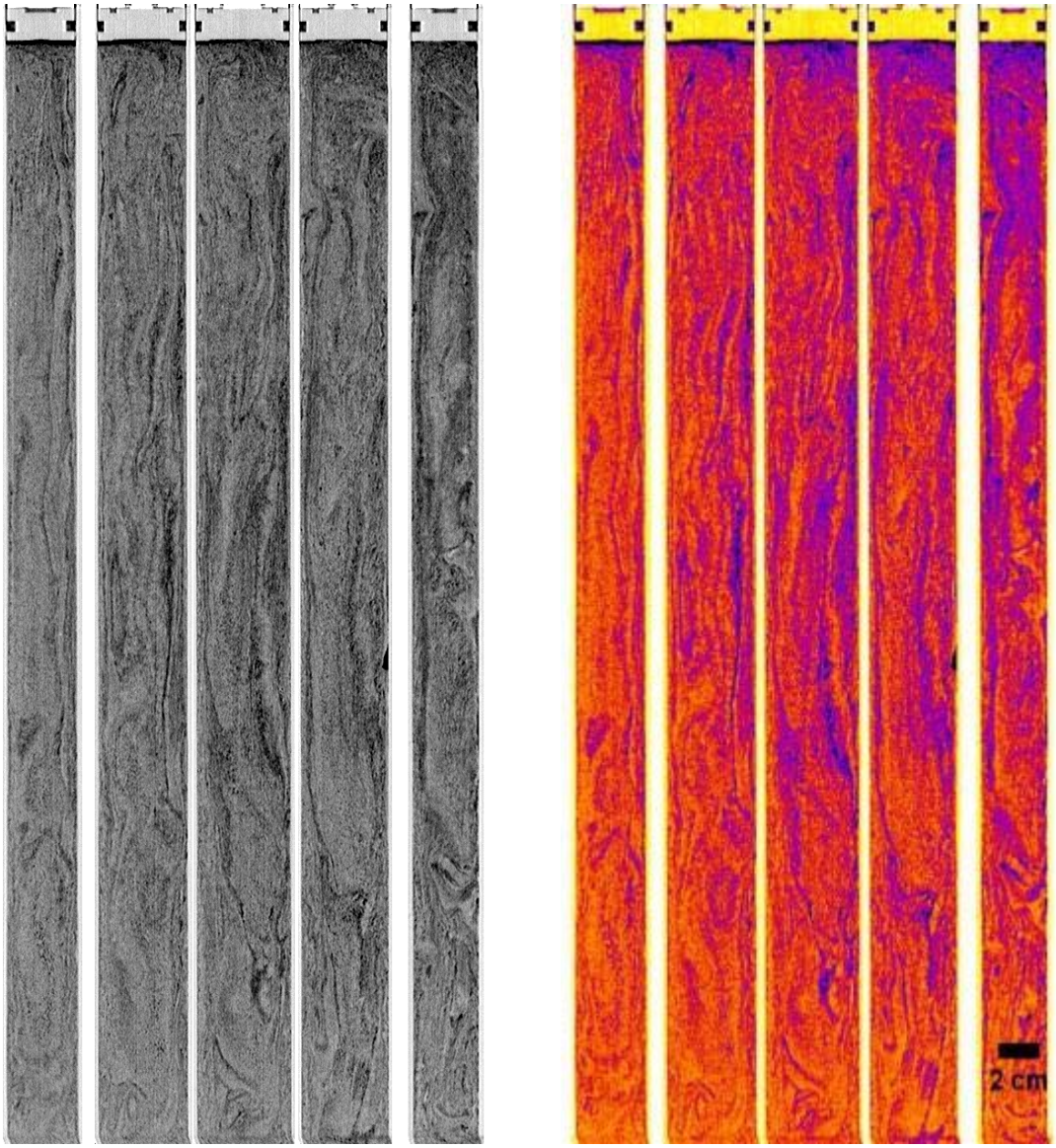

Figure 6: Reconstructed medical CT images of aluminum vessel D1. Each image is a montage of five cross-sections through XZ planes of the vessel. Left: grayscale rendering. Right: false color images. Estimated foam quality 41.2% (Table 1).

The volume of higher porosity zones in the CT images shown in Figure 6 appears to increase from the injection port (on the bottom) to the retracting piston (on the top). To evaluate this, the average CTN within a 13.8 cm^2 (2.1 $in.^2$) circular area region of interest (ROI) was measured at each XY plane along the length of the vessel. The resulting plot, shown in Figure 7, reveals that the CTN does decrease along the flow length of the vessel, indicating an increase in the gas fraction at the top of the sample. The rapid decrease in CTN near the retracting piston at 53.3 cm (21 in.) indicates a similar phenomenon to what was observed in the steel A1 sample; a small gas-filled region at the top of the sample. The overall size of the "gas cap" in sample D1 is smaller than in the A1 sample, less than 1 cm (0.4 in.).

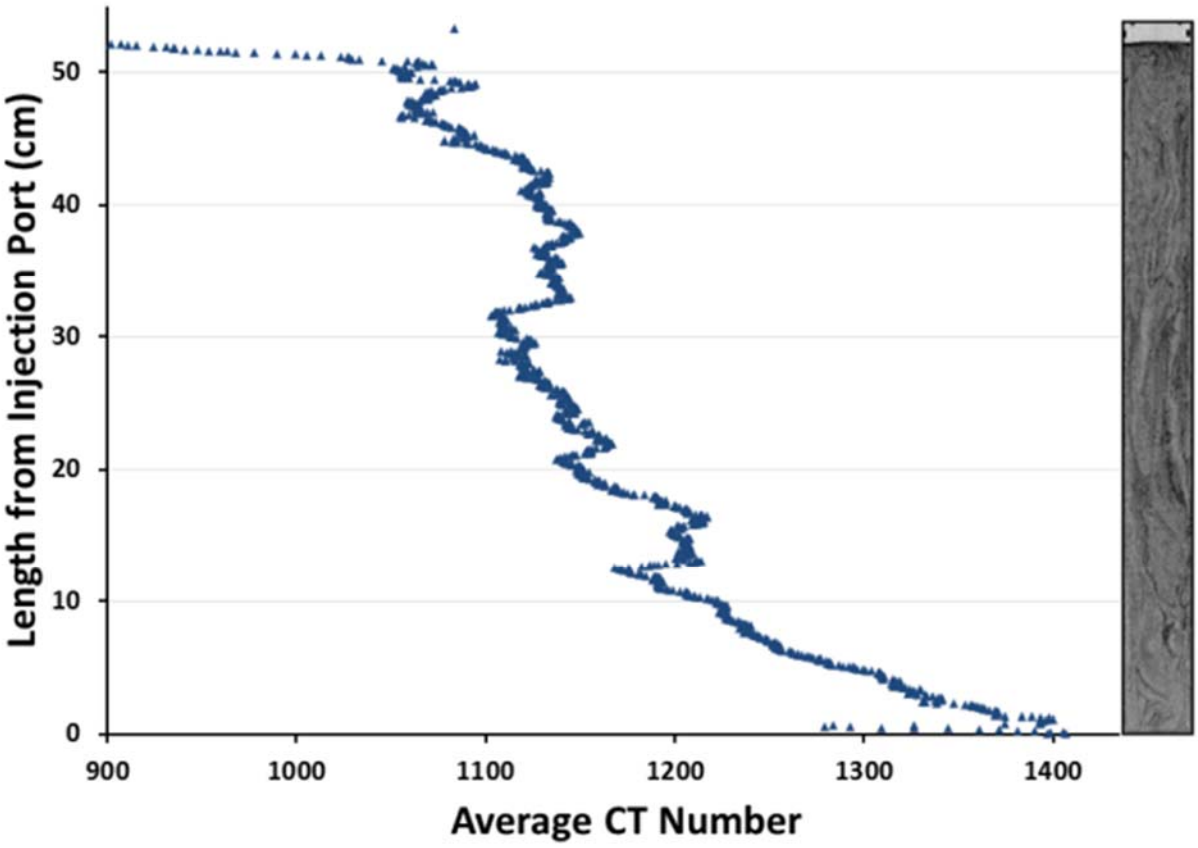

Figure 7: Average CT number of a 13.8 cm^2 (2.1 in.^{2}) area through the center of pressurized sample D1 along the vessel length. Lower CT number indicates a lower density (higher gas fraction). An XZ grayscale slice through the center of the vessel is shown adjacent to the plot.

Several histograms of the CTN within a 12.5 cm^2 (1.9 in.^{2}) area ROI were plotted along the length of the core as well. As is shown in Figure 8, the distribution of CTN near to the injection port (6.25 cm) is narrower than the distribution near the top of the vessel (50.0 cm). This indicates that the foamed cement has a more uniform density near the injection side and has a wider range of high and low porosity zones towards the top of the sample vessel, as can be visually discerned in the full length XZ montages in Figure 6. In addition, XY grayscale slices of the cement at distances 6.25, 18.75, 31.25, and 50.0 cm from the injection port where these measurements were performed are shown in Figure 8. Fewer low porosity zones are apparent in the slice closest to the inlet, with an increasing number of distinct low porosity zones towards top of the vessel.

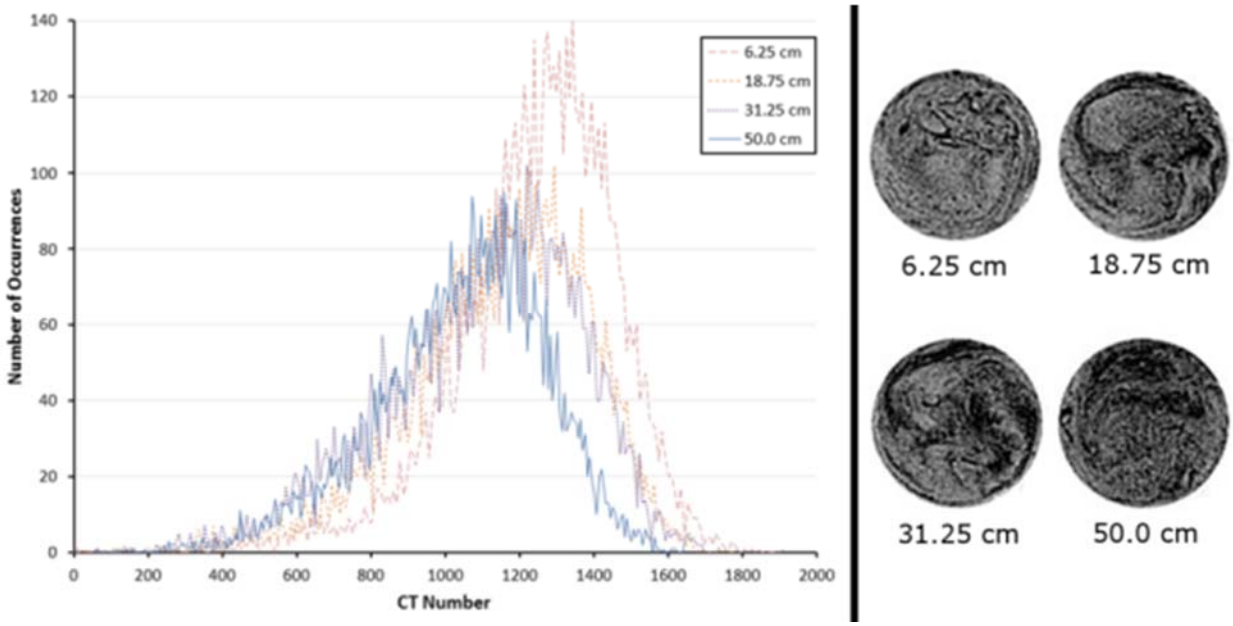

Figure 8: Histograms of CT number within a 12.5 cm^2 (1.9 in.^{2}) area through the center of pressurized sample D1 along the vessel length. Labels indicate distance from the injection port. XY grayscale slices show measured CT images.

Unlike the higher resolution industrial CT scans of atmospherically-generated foamed cement (Kutchko et al., 2013, 2014) the distribution of CTN from the medical CT scans is not bimodal with obvious CTN value ranges for gas and cement. The majority of the bubbles within the foamed cement are below the voxel resolution of the medical scanner. Even though these small bubbles cannot be directly imaged they produce a localized reduction in the CTN because voxels are partially filled with gas, i.e. partial volume effects (Keller, 1997). This makes the isolation of low porosity regions from the medical scan more difficult. An attempt to isolate the low density zones within the D1 pressure vessel by applying a threshold is shown in Figure 9. Several differences in the structure of these low density zones can be identified. The bottom quarter of the sample has relatively few low density zones. The middle half of the vessel is dominated by elongated low density structures. These structures appear to be partially connected and follow "wavy" patterns. The upper quarter of the cement has elongated low porosity structures, but also has more dispersed low porosity zones. The complexity of the structure within this one CP vessel indicate that localized, small-scale analysis of the BSD within the field-generated foamed cement samples may not capture the entirety of the pertinent information about foamed cement generated at "'one condition" or "one quality".

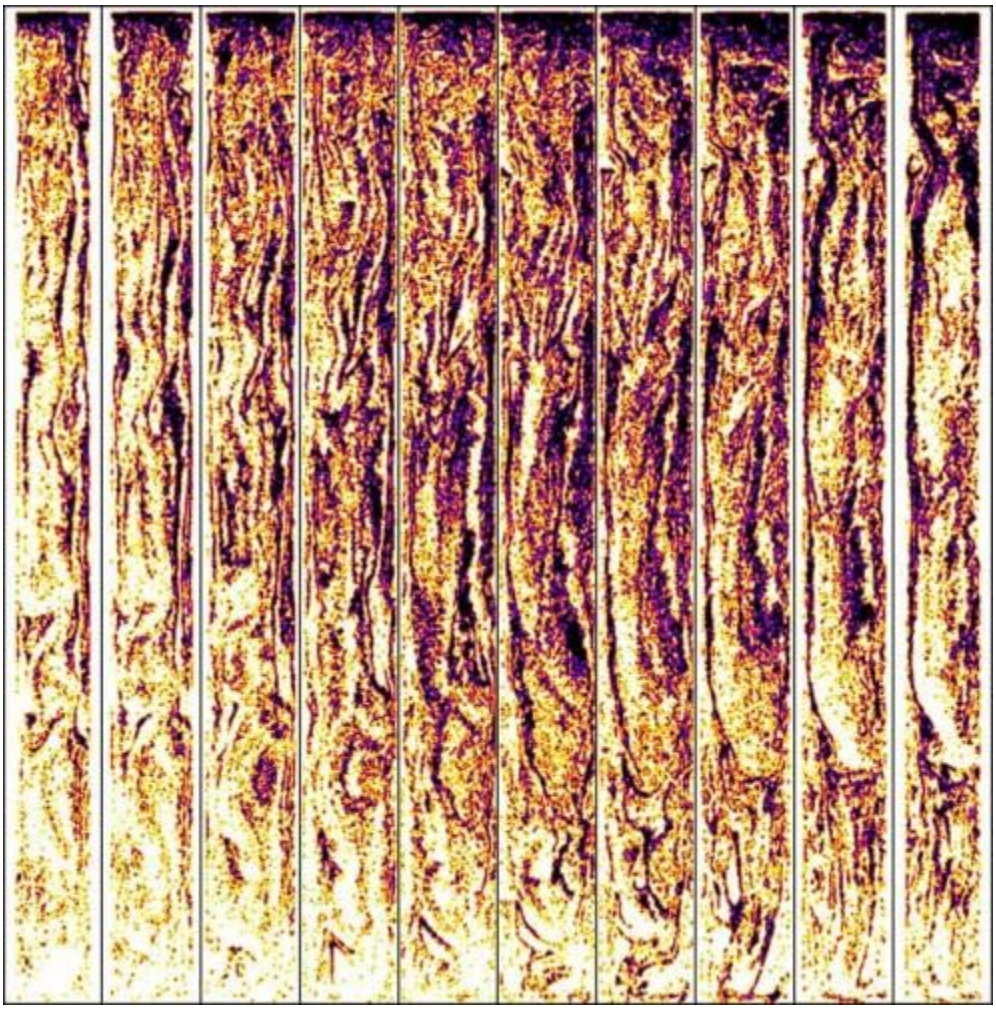

Figure 9: False color XZ slices of pressurized vessel D1 with a threshold applied to isolate low CTN (i.e. low density) zones, which are shown as darker regions.

Next, the sample was imaged in the industrial CT scanner, with a voxel resolution of ~ $(35\ \mu m)^3$. A segment of CT Sample D1 showing low density isolated zones (white) and individual voids (red) are shown in Figure 10. The connected nature of these structures is visible in Figure 11.

Industrial CT scans permit a more detailed analysis of the structure of the foamed cement samples. Figure 10 is a segment of sample D1 showing low density isolated zones (white) and individual voids (red) as examined in the industrial CT scanner (voxel resolution of ~ $(35\ \mu m)^3$). Figure 11 is a 3-D representation of several 2-D slices of sample D1. Low density regions of cement (i.e. the dark zones) where cement is more porous can be seen in the false color slices in Figure 11. There appears to be a strong linkage between structures observed and the flow of the cement; detailed analysis of this behavior is on-going.

Figure 10: Industrial CT scans of sample D1. Low density zones are shown as white, while high density zones are shown as red.

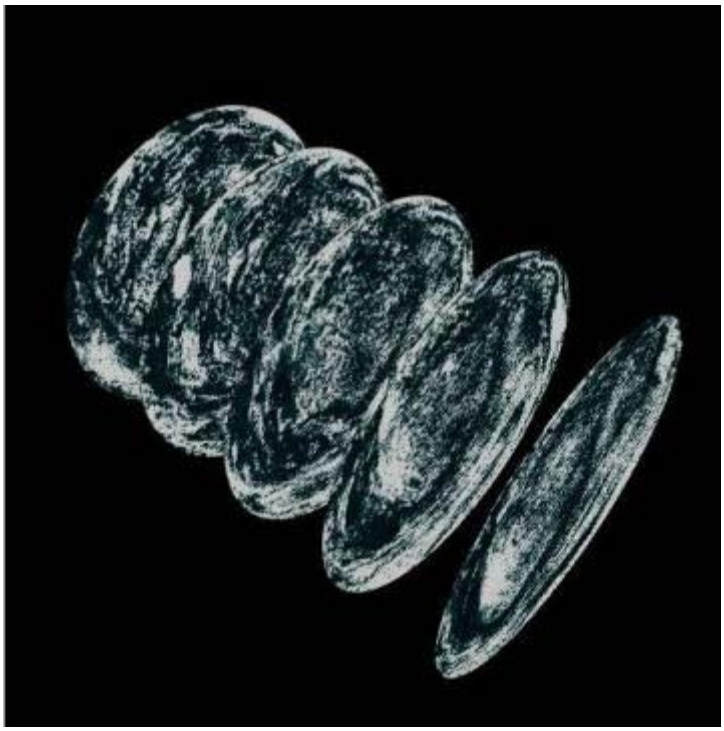

Figure 11: Montage and ortho-slices showing low density regions along a segment of sample D1.

3.3 SAMPLE D2

Pressurized aluminum sample D2 was scanned and XZ montages of this vessel are shown in Figure 12. Visual examination of these slices indicates that there are fewer distinct low density structures within this sample, as compared to sample D1. The amount of free gas adjacent to the piston at the top of this sample is larger than D1; roughly 1.3 cm (0.5 in.) of space is gas filled. This sample does appear to be somewhat more homogeneous along the vertical axis, which is also shown by the CTN variation along the length of the vessel shown in Figure 13. For these measurements a 12.0 cm^2 (1.9 $in.^2$) ROI was used and the resulting change in CTN was less than 200 across the entire core, which is less variation than was seen in the similar analysis of D1, where the CTN was roughly 350 less at the top of the vessel when compared to the entrance. In addition histograms of the CTN variation of four CY slices along the length of the sample vessel (Figure 14) reveal that the distribution of high and low density regions along the length of the core is quite similar throughout the length of the vessel. Similar to what was observed in sample D1, the histogram of the XY slice closest to the injection port (6.25 cm) shown in Figure 14 has a narrower distribution, but unlike sample D1 the remaining distributions of CTN along the length are similar.

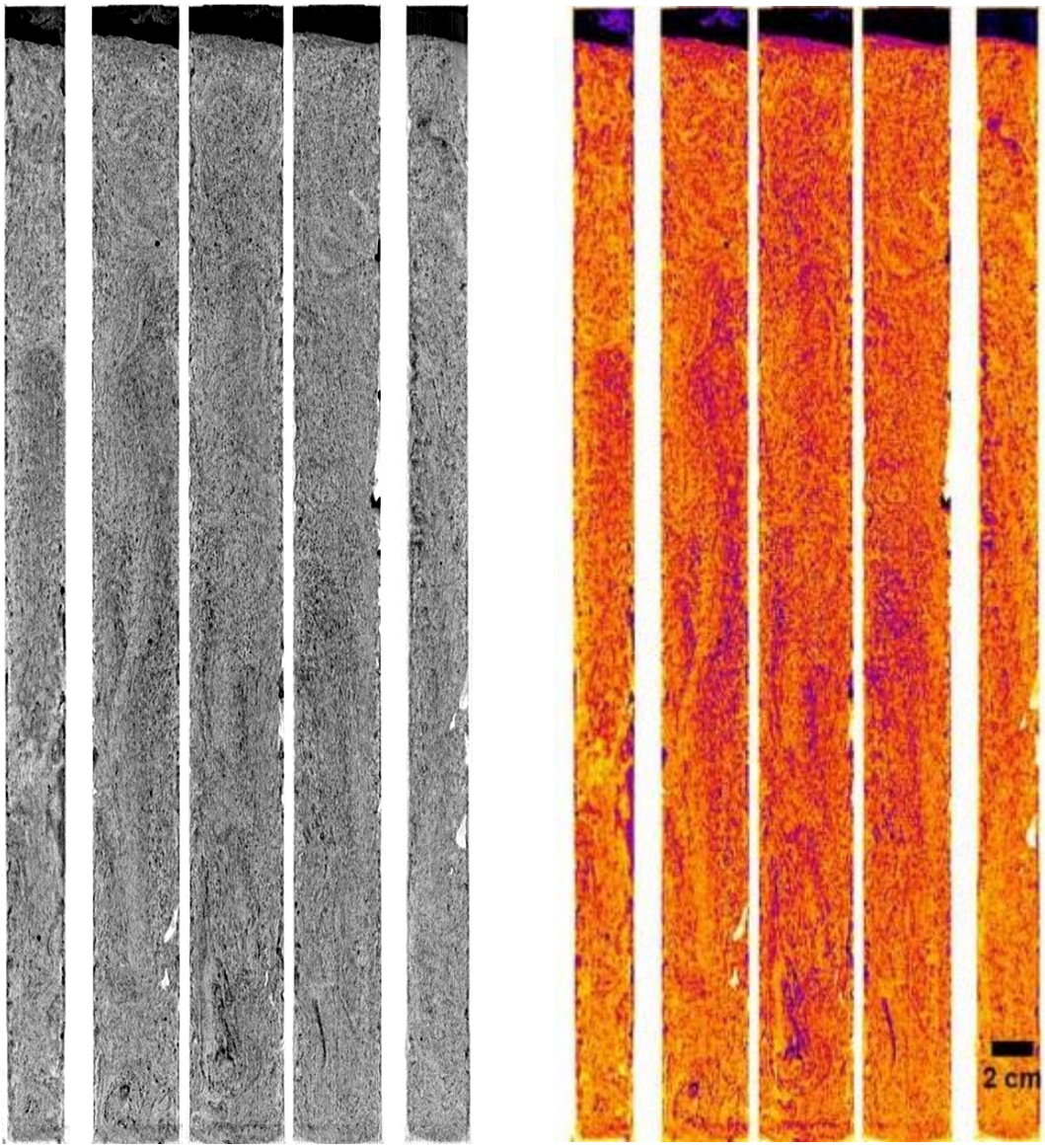

Figure 12: Reconstructed medical CT images of aluminum vessel D2. Each image is a montage of five cross-sections through XZ planes of the vessel. Left: grayscale rendering. Right: false color images. Estimated foam quality 47.3% (Table 1).

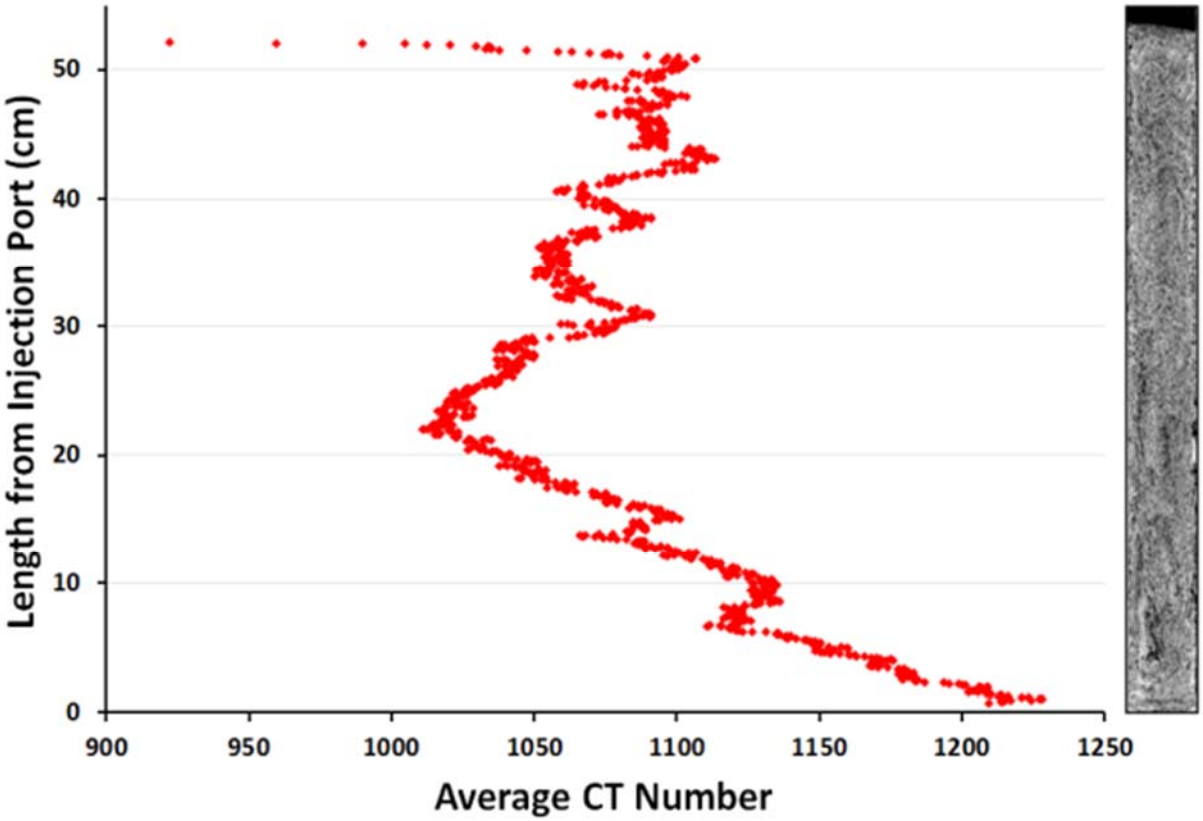

Figure 13: Average CT number of a 12.0 cm^2 (1.9 in.^{2}) area through the center of pressurized sample D2 along the vessel length. An XZ grayscale slice through the center of the vessel is shown adjacent to the plot.

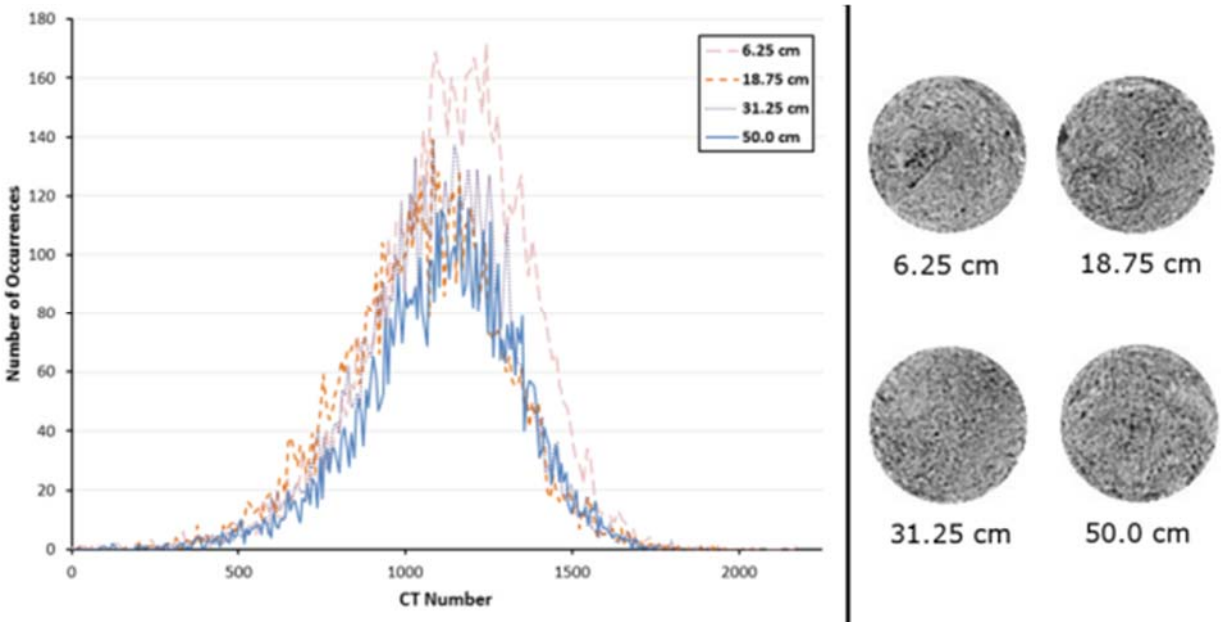

Figure 14: Histograms of CT number within a 13.7 cm^2 (2.1 in.^{2}) area through the center of pressurized sample D2 along the vessel length. Labels indicate distance from the injection port. XY grayscale slices show measured CT images.

Even though sample D2 is more uniform than sample D1 there is a distinct distribution of low density zones throughout the vessel. These are best visualized in 3-D and are shown in Figure 15 where a 3-D rendering of the entire core is shown along with a 3-D representation of low density zones that have been isolated with an Otsu threshold technique using ImageJ. 3-D renderings of the core without low density zone isolations are shown in Figure 15 (A) and (B). An Otsu threshold procedure was run on the sample to isolate the lowest CTN values, which correspond to the lowest density zones, from the original grayscale distribution. The 3-D rendering of these zones is shown in Figure 15 (C) and (D). Near to the injection port (bottom right of the images in Figure 15) the low density zones appear to start as a small connected "stream" which grows as it propagates up the vessel. Roughly one third of the way up from the bottom of the vessel the low density zone bifurcates into two larger zones that follow the edge of the sample container. This region corresponds well with the reduction in CTN between 14 and 25 cm (5.5 to 9.8 in.) from the injection port of the vessel, shown in the average CTN along the length in Figure 13. The top 25% of the sample has less of a continuous low density zone structure, with more dispersed regions of low density cement. These renderings appear to show that a "connected" structure of low density cement formed during the collection process in the CP sample containers. Because of the low resolution of the medical CT scans, it cannot be inferred that these regions contain connected bubbles that could form preferential pathways, but rather these regions seem to indicate preferential clustering of bubbles within the domain.

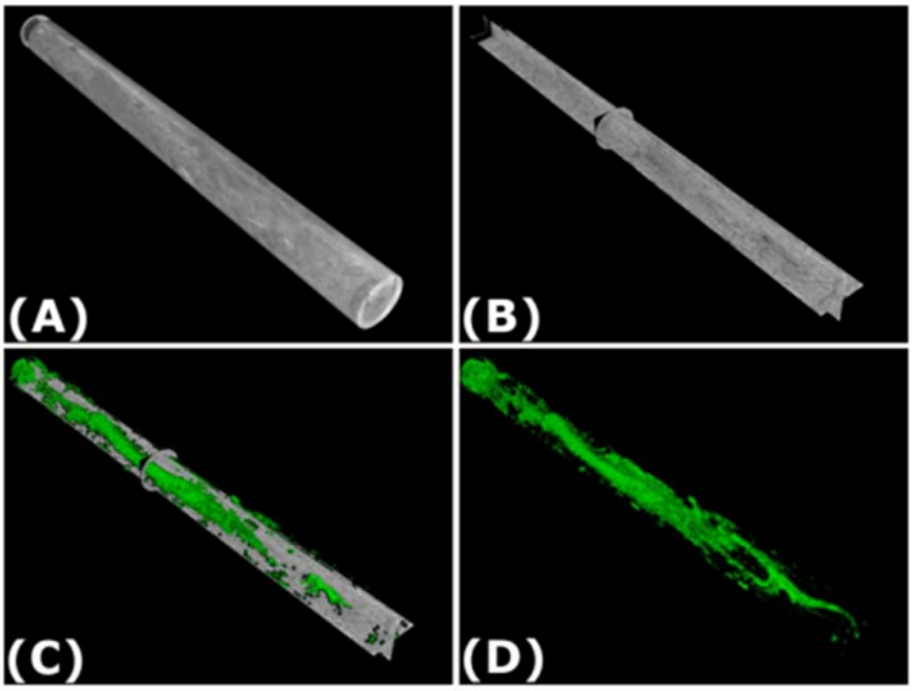

Figure 15: 3-D reconstructions of pressurized sample D2. Injection port is in the bottom right of each image; retracting piston in the top left. (A) 3-D reconstruction of entire sample. (B) Orthoslice along the primary directions of the vessel. (C) Othoslice and 3-D rendering of isolated high porosity zones. (D) 3-D rendering of just the high porosity zones.

3.4 SAMPLE E1

Pressurized aluminum sample E1 was scanned and XZ montages of this vessel are shown in Figure 16. This sample is distinctly different than the other three samples. A significant amount of higher density cement is observable within this sample, as shown by the brighter/lighter regions in Figure 16. This appears to follow the edge of the vessel in the third of the vessel closest to the injection, and distributed throughout the sample in the top half of the cement. There is a large 4.9-cm (1.9 in.) long void space adjacent to the retracting piston, but careful examination of the images reveals that this is filled primarily with a lower density liquid when it was scanned. As shown in Figure 17, a meniscus of fluid can be seen in the sample vessel, which was laid on its side to perform the medical CT scanning. This is likely fluid/solids separation, an expected consequence of the high foam quality captured in the sample collection. There are also a number of air voids large enough to be discerned by the medical CT scan throughout the sample.

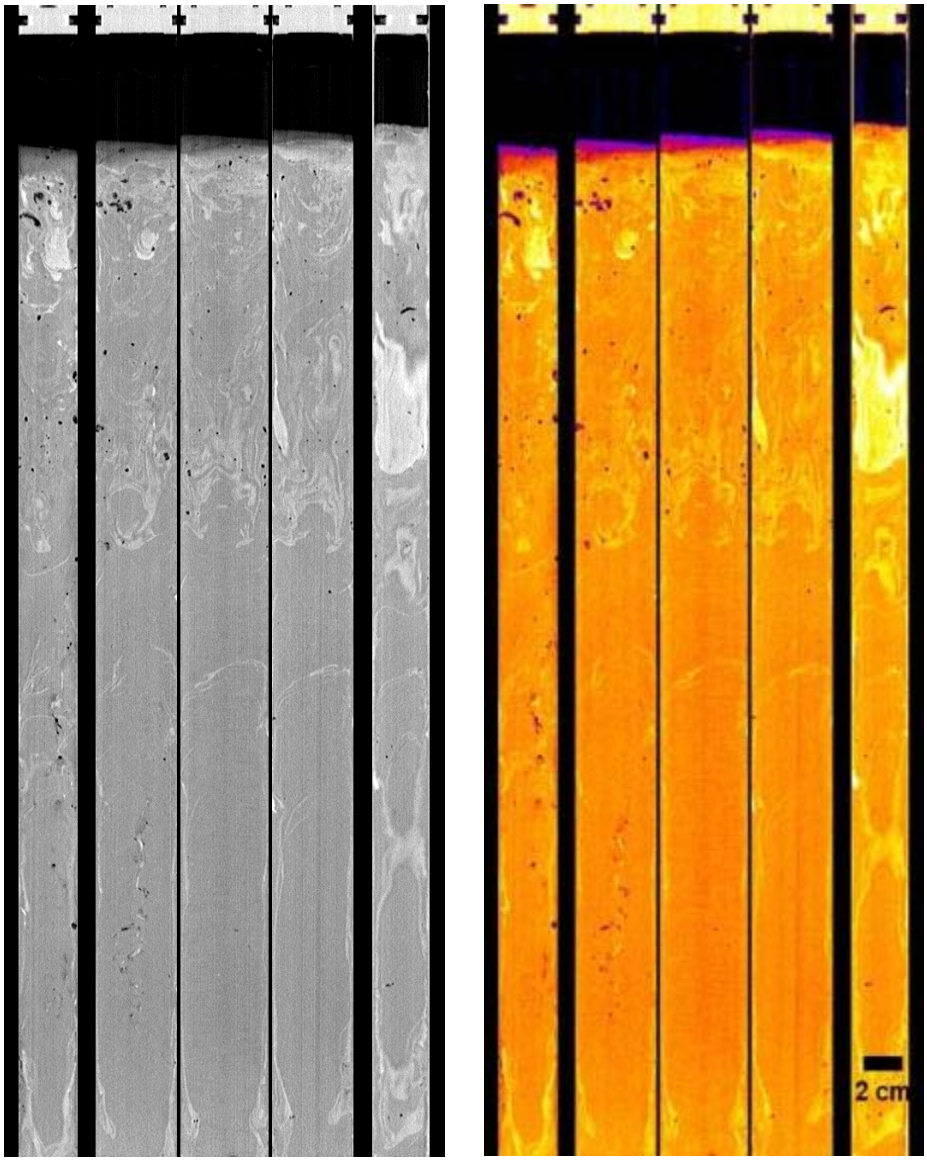

Figure 16: Reconstructed medical CT images of aluminum vessel E1. Each image is a montage of five cross-sections through XZ planes of the vessel. Left: grayscale rendering. Right: false color images. Estimated foam quality 31.5% (Table 1).

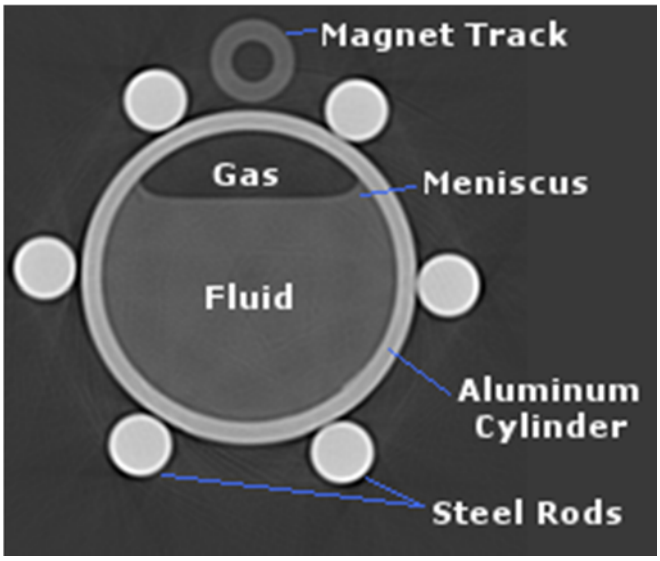

Figure 17: XY slice of the entire E1 CP vessel 53.3 cm (21 in.) from the injection port. Labels identify the parts of the CP sample vessel and the fluid/gas interface of within the non-cemented zone at the top of the vessel.

Figure 18 is a plot of the average CTN in a 14.2 cm^2 (2.2 $in.^2$) circular ROI along the length of CP sample vessel E1, with a XZ grayscale slice through the center of the vessel shown above the plot for reference. The variation along the length of the sample is different than that observed with the other aluminum vessels in that the density at the top of the sample is actually the highest in the entire sample. The CTN does decrease for the first 8 cm (3.1 in.) above the injection port, and then there is a fairly stable zone of constant density between 12 and 26 cm (4.7 and 10.2 in.), but above this the average density increases significantly. This bulk density increase is due to the high density zones visible at the top of the sample as seen in Figure 16.

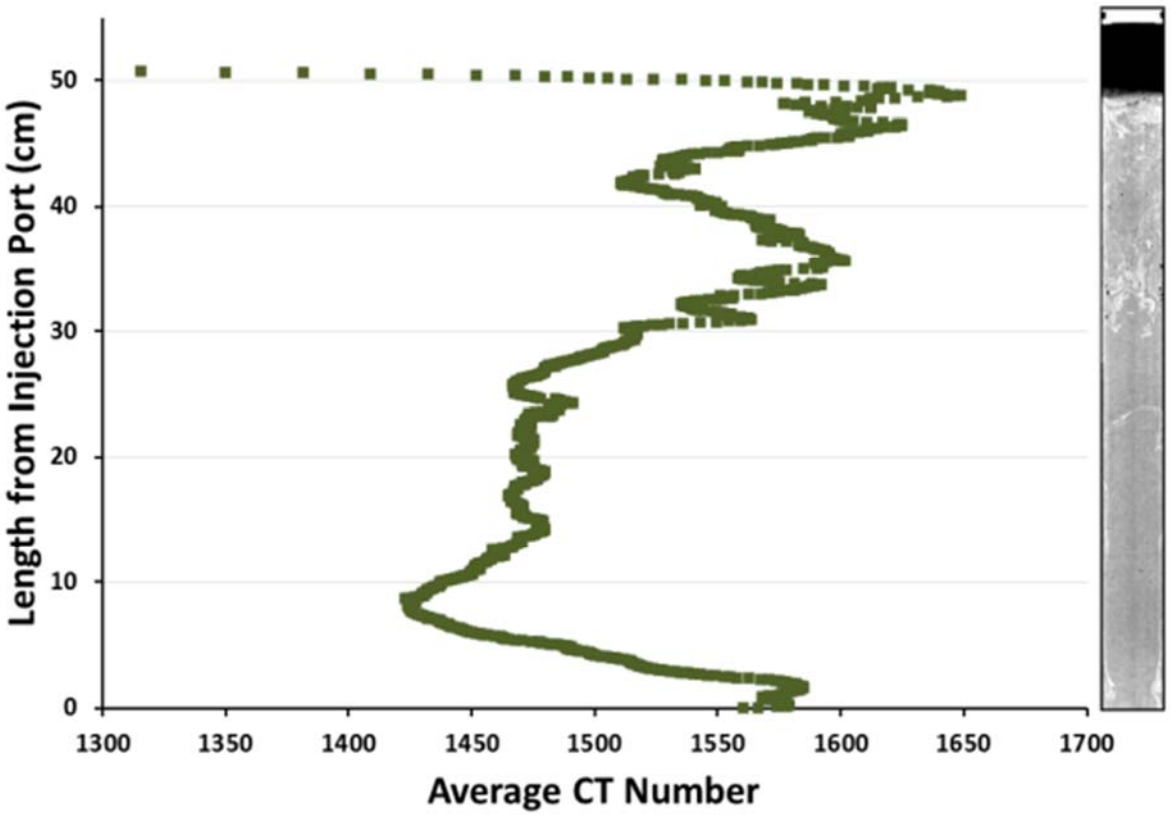

Figure 18: Average CT number of a 14.2 cm2 (2.2 in.^{2}) area through the center of pressurized sample E1 along the vessel length. An XZ grayscale slice through the center of the vessel is shown adjacent to the plot.

Histograms of the CTN at four locations along the length of sample E1 are shown in Figure 19. The distribution of CTN at 6.25 cm from the injection is similar to what was observed in samples D1 and D2, with a fairly narrow and focused range of CTN values. In the center of the sample at 18.75 and 31.25 cm the CTN values increase, shifting the distribution to higher CTN values, but remaining fairly focused around a narrow range of CTN values. At 50.0 cm from the injection port the CTN distribution widens significantly, indicating a larger mix of both high and low density cement at the top portion of this sample.

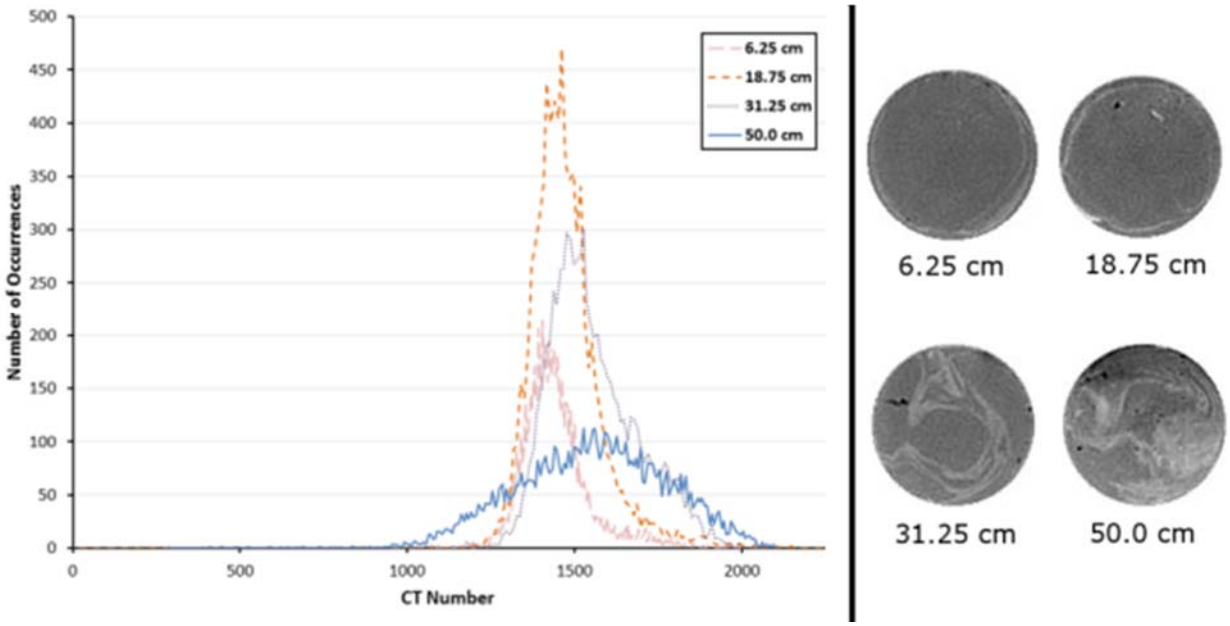

Figure 19: Histograms of CT number within a 14.2 cm^2 (2.2 in.^{2}) area through the center of pressurized sample E1 along the vessel length. Labels indicate distance from the injection port. XY grayscale slices show measured CT images.

Two thresholds of the CT scans of sample E1 were performed to isolate the high and low density regions within the CP sample vessel. Figure 20 is a montage of 15 of XZ planes through the container with the low density zones shown in green and the high density zones shown in blue. The liquid and gas filled region adjacent to the retracting piston is readily apparent as a low density zone, but large air voids are seen distributed throughout the cement as well. Most of the large air voids appear around the high density zones in the upper third of the cement. There is apparently a complex interaction of high density zones with the large air voids, perhaps where the bubbles in the foamed cement have collapsed. Understanding why this sample behaved so differently when the sampling procedure was nearly identical from test to test may help to better describe foamed cement stability within borehole applications.

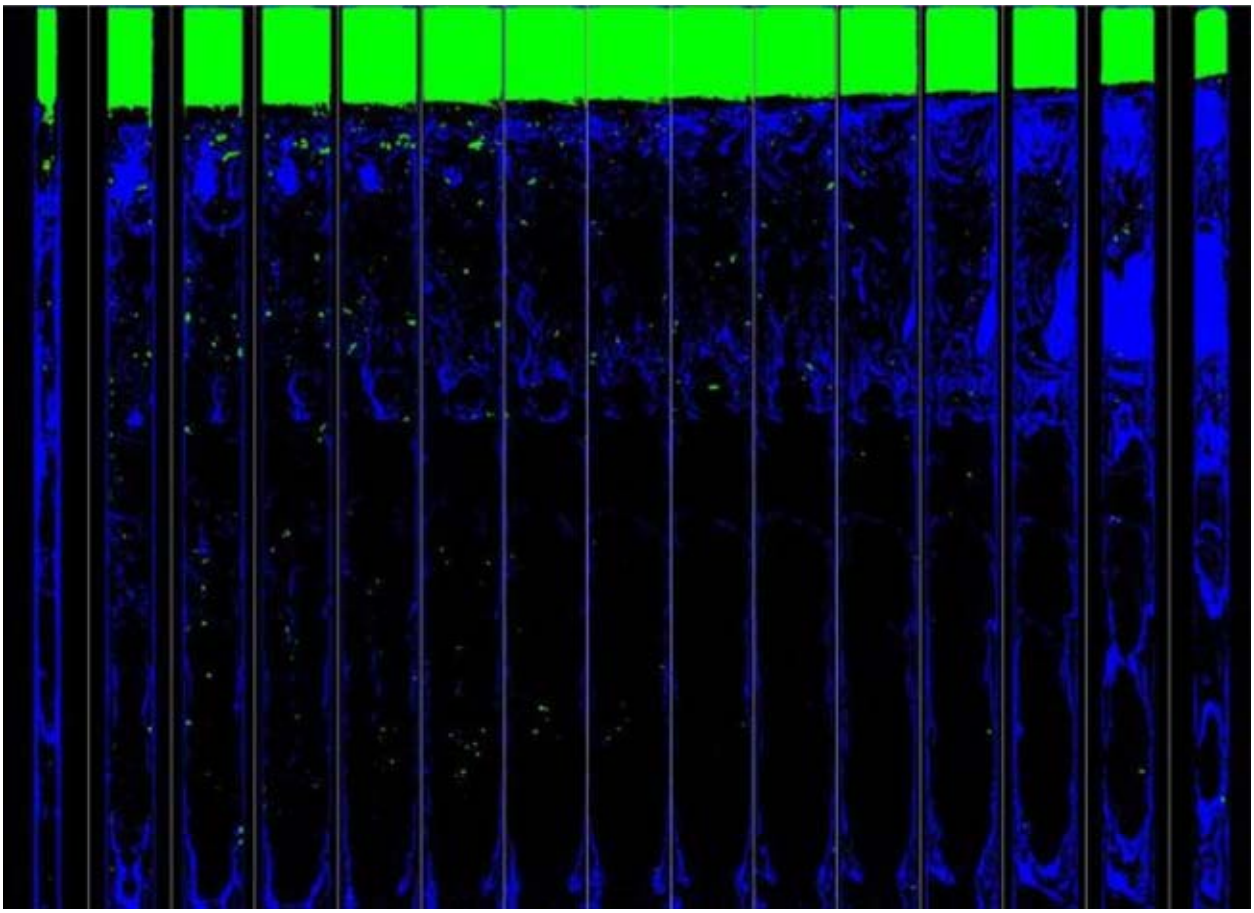

Figure 20: False color XZ slices of pressurized vessel E1 with a threshold applied to isolate low and high CTN/density zones. Low density zones are shown as green, while high density zones are shown as blue.

The industrial CT scanner lacks the ability to scan large areas like the medical CT scanner. However, the industrial CT scanner has a higher resolution with the ability to generate images with cubic voxel resolutions from 10's of microns per voxels, even as low as in the single digits, depending on scanning techniques used. Although the scans took much longer, discrete bubble distributions, as well as minor and major features, were visible due to the much enhanced resolutions.

Sample E1 was scanned with the industrial CT scanner at a voltage of 185 kV, a current of 400 μA, and an exposure time of 500 ms. The acquired voxel resolution was 35.7 μm^3.

The images from industrial CT scanning were processed with ImageJ (Rasband, 2012). Tiff image files were read into ImageJ as a stack of XY slices for each scan. Due to the limited area available in the industrial CT scanner, each sample was scanned along multiple transects, up to 9, to encompass the full scope of the samples. Each subsection was treated as a separate sample with full image processing and analysis performed.

Figure 21 is a combination of eight separate scans of the pressurized aluminum E1 sample that are grayscale blended and enhanced with contrast adjustment. The sample is heterogeneous as was shown by the medical CT scanner; however, resolution improvements via the industrial CT

scanner allow for detailed analysis of the structures. The outside of the vessel has higher density regions, illustrated by lighter greys, with variable density changes throughout. The inlet is observed in Figure 21 (A) where the metal cap and port hole are exposed. Gas bubbles accumulated near the top of the core as shown in Figure 21 (B), and were angled because the sample was titled during the curing. Figure 21 (C) and (D) illustrate a density separation, where two additional phases denser than B are present, with (C) having a more homogenous and non-porous character and (D) having a more porous character. These features are unique in that they are preferentially above a less dense phase, indicating that the buoyancy forces in the gas phase of zone (B) were not sufficient to allow vertical transport through the material in zones (C) and (D) to the top of the core.

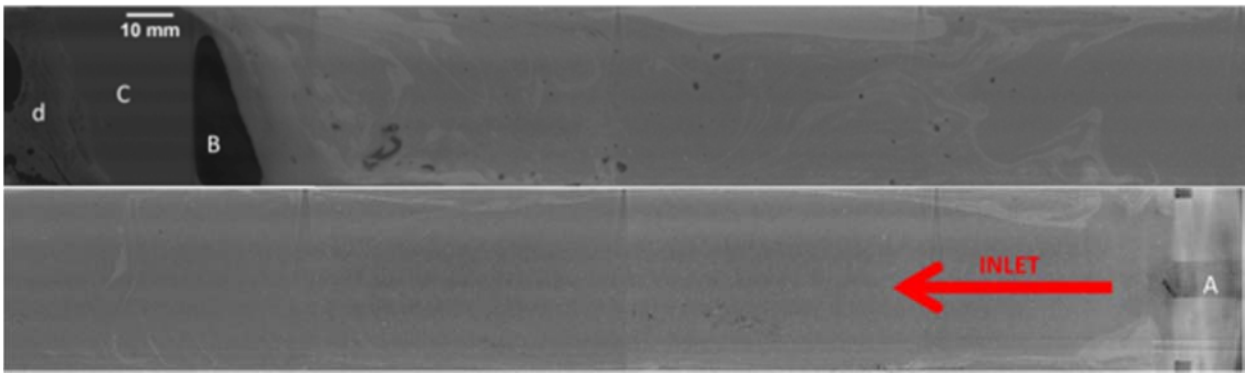

Figure 21: View of the entire E1 core sample spliced together; inlet direction also indicates flow direction with bottom half representing the intial entry and the top half representing the upper-most section of the sample. (A) Indicates inlet where cement first enters vessel, (B) gas pocket, (C) lower density media, and (D) lower density "bubble" media.

A more enhanced view of E1 with the top one third section, shown in Figure 22A, highlights some of the flow structures within the core. Dense regions (white) where cement is less porous can be seen in the false color slice in Figure 22B. One macro-void, which is less dense, shown in Figure 22C–E is unique in that it exhibits a "corkscrew" shaped structure. This structure may be indicative of a localized flow eddy. The structure is the only such structure definitively isolated in the core; however, it appears that similar smaller structures exist throughout.

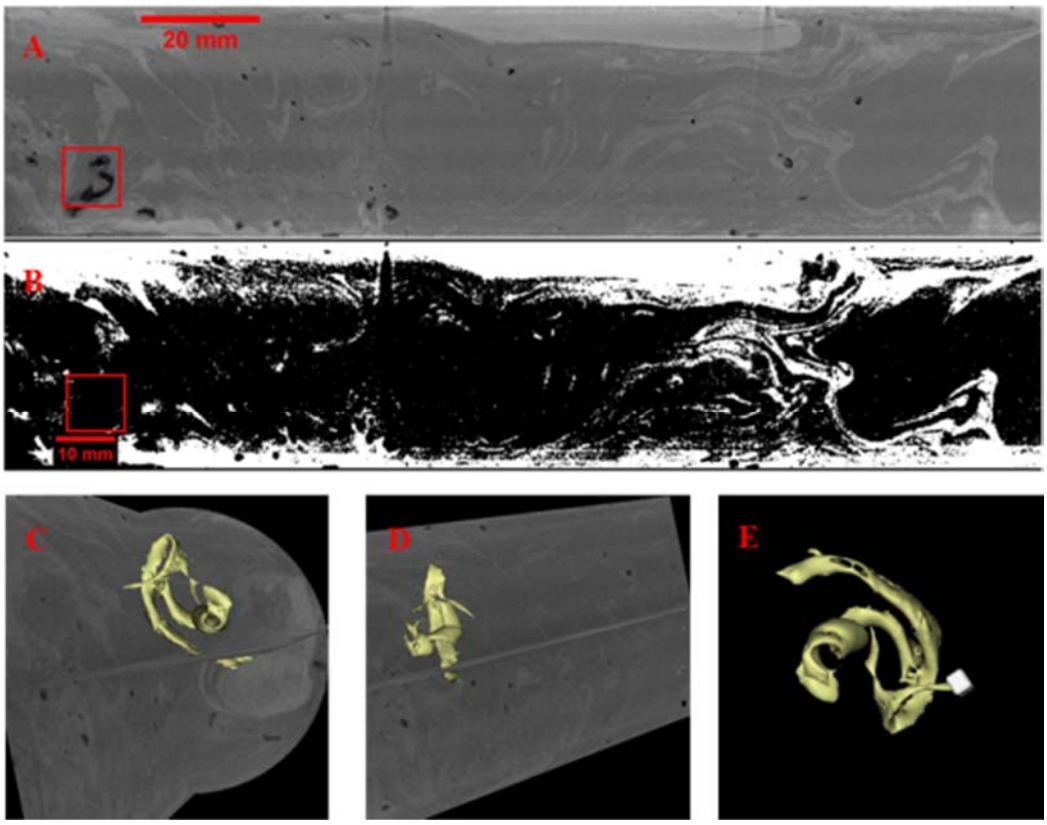

Figure 22: (A) XZ slice of pressurized vessel E1 - bottom third of the vessel, (B) XZ slice of E1 thresholded to illustrate flow structure where white indicates more dense material, (C–E) Low density "corkscrew" structure displayed in ortho perspective, C and D, and freeform beside a 1 mm^3 cube. Red highlight box represents area where "corkscrew" feature is located in whole core.

Sample E1 was scanned and initial analysis of the XZ planes of these scans appeared to indicate linear bands of flow disturbance, possibly due to shearing of the foamed cement slurry near to the vessel walls (Figure 23). Further investigation, in 3-D (Figure 24), shows that the structure is actually a helical-shaped dense disparity in the matrix. It is notable that the helix structure is comprised of more dense material (white) surrounded by less dense matrix material and interspersed voids, which suggests that this structure may be due to the settling of a more dense material after foamed cement flow ceased. This hypothesis is supported by the structure being compact near the top of the structure and more dispersed near the bottom, as if dense zones spread out as they settled through the slurry. It is possible that these structures are a by-product of sampling methodology and further comparisons will need to be conducted before a definitive conclusion can be drawn as to the nature of the objects in Figure 23 or Figure 24.

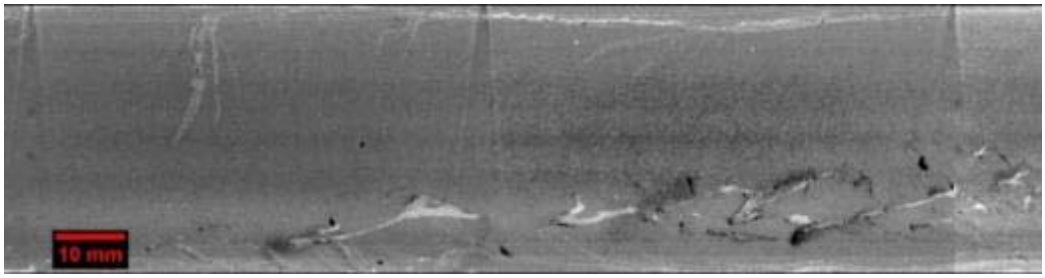

Figure 23: XZ slice of pressurized vessel E1 – middle third of vessel showing linear dense bands.

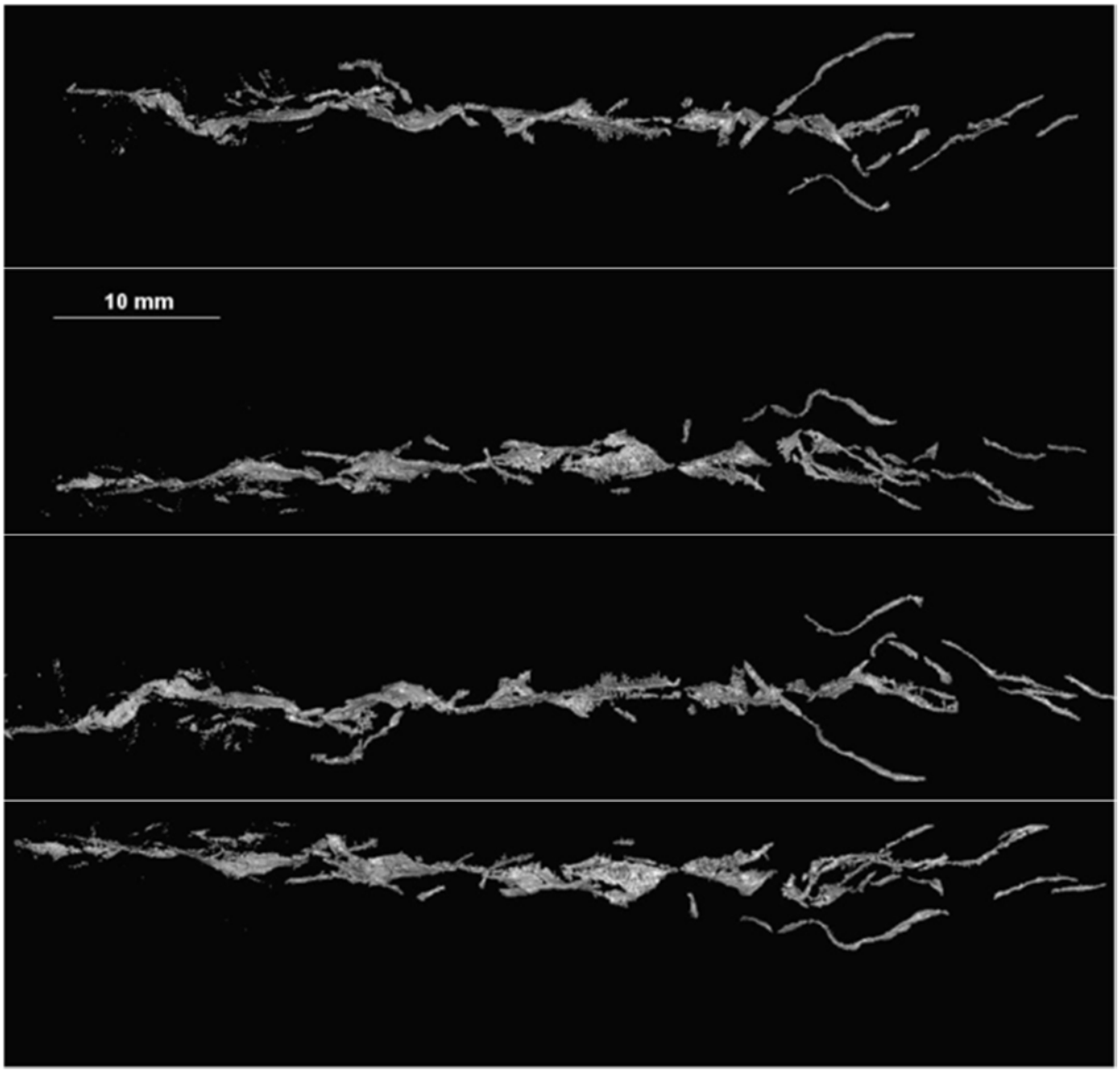

Figure 24: Separate 90º views of large helical structure from E1. Flow is from right to left, with the right end being closer to the inlet.

At the inlet orifice gas and liquid filled voids were observed. These are shown as red and blue voids for the gas and liquid filled voids in Figure 25, respectively. These regions likely formed as the cement was entering the pressurized vessel. The abrupt change in geometry may have resulted in this unique distribution of irregularities; alternatively closing of the valve after filling may have preferentially allowed less viscous materials, such as gas and water slurry, to enter into the vessel. Further analysis of the effect of changing geometries on the creation of macro voids is underway using the FCG in the laboratory at NETL Morgantown, WV.

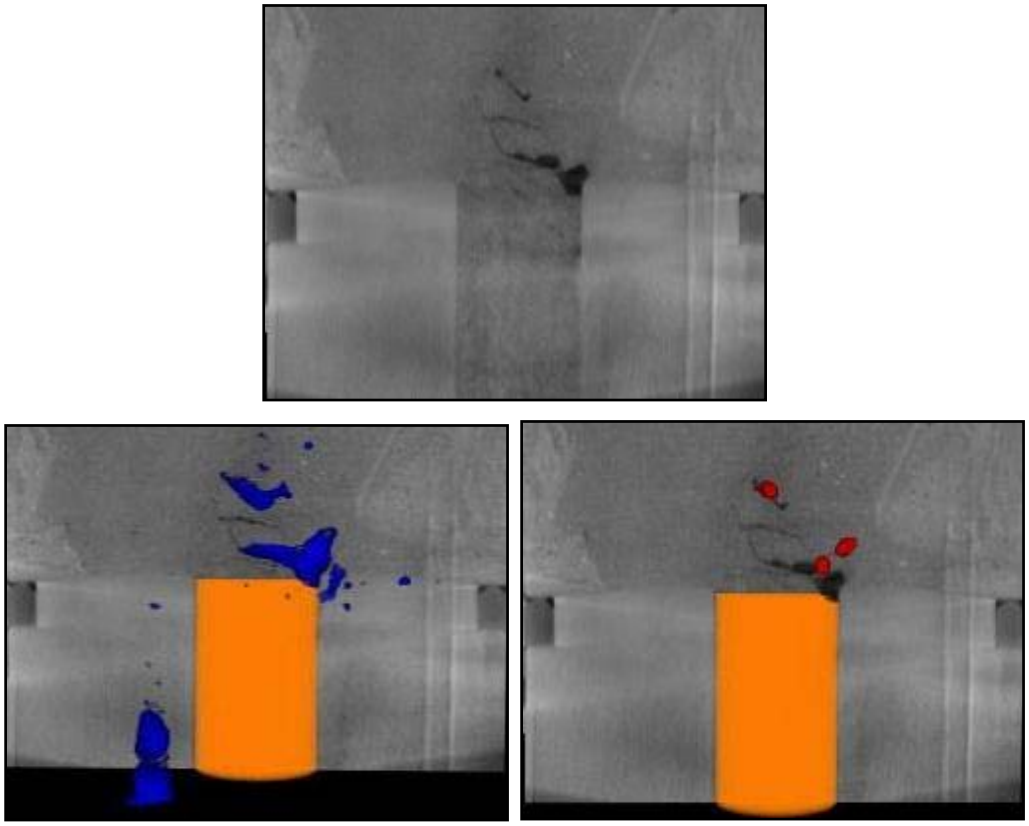

Figure 25: Structures adjacent to the inlet of sample E1. Top, greyscale slice through the inlet. Bottom left, isolated gas filled voids near inlet in blue. Bottom right, isolated liquid filled voids near the inlet in red.

4. DISCUSION

The novel collection process of pressurized foamed cement has enabled an unprecedented examination of foamed cement structures. This collection methodology revealed a heterogeneous void distribution within each of the cement samples and variations between the different samples as well. Samples D1 and D2 had similar distributions of density over the length of the vessels, with higher density cement near to the inlet. Sample E1 was more uniform and had a higher density throughout the entire length of the vessel than the other two samples. Figure 26 is an illustration of the differences in the CT number (a proxy for density) observed between the three samples.

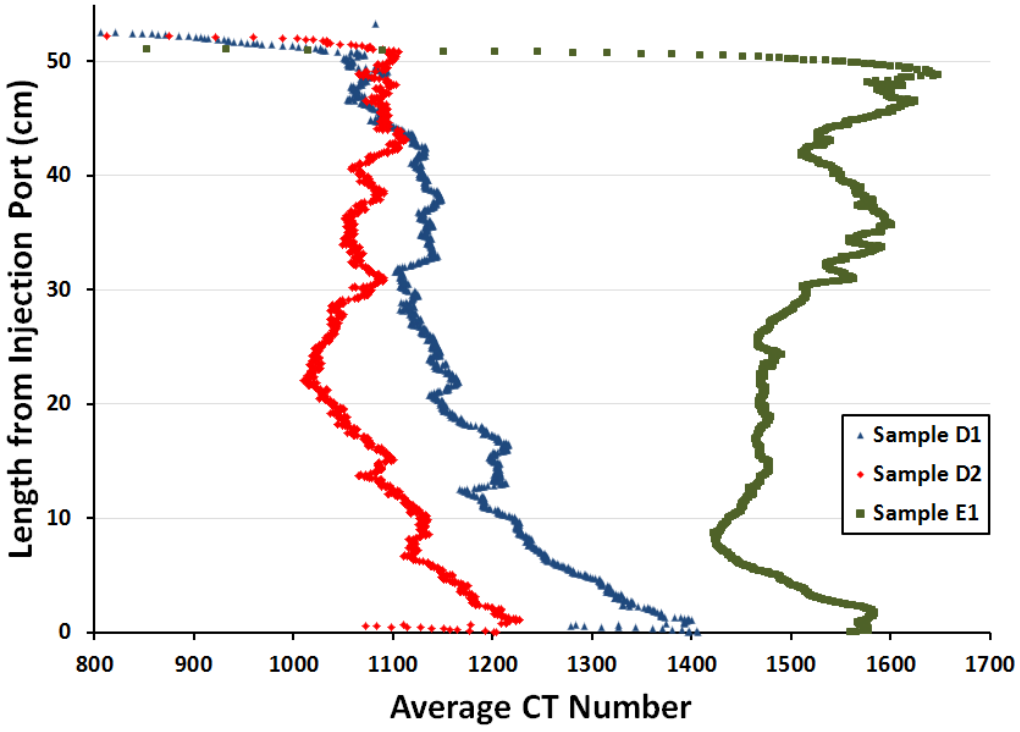

Figure 26: Average CT number through the center of the three pressurized samples along length of the vessels.

As previously stated, many of the localized low density swirl-zones are reminiscent of particle clustering in low vorticity zones found in turbulent flows (Nasr et al., 2009). To examine whether this is a viable hypothesis the Reynolds number (Re) of the flowing foamed cement in the vessel was estimated. Re is the dimensionless ratio of inertial to viscous forces and is defined as (White, 1999)

$$\mathrm{Re} = \rho UL / \mu \tag{1}$$

where ρ is the fluid density, U is the fluid velocity, L is a characteristic length scale, and μ is the absolute viscosity of the fluid. The determination of exactly what Re constitutes turbulent flow varies depending on many environmental variables, such as surface roughness, but within a pipe

the critical value above which turbulent flow is expected is typically assumed ≈2,300 (White, 1999).

A video of foamed cement vessel D2 being filled was captured and the movement of the magnet moving up the external track was used to estimate a U ≈ 0.0154 $^{m}/_{s}$. The inside radius of the vessel was used as L = 0.0254 m. Assuming a neat cement slurry density of 1442 $^{kg}/_{m^3}$ and a gas quality of 47.8% (Table 1) yields a foamed cement ρ ≈ 752.7 $^{kg}/_{m^3}$. The μ was estimated from the experimental results presented in Ahmed et al. (2009) for 30% quality foamed cement undergoing a shear rate of 600 s^{-1} (which is the largest shear rate with the highest quality foamed cement examined by Ahmed et al. (2009)) as 0.3 Pa*s. Using these values to estimate Re from Equation 1 yields Re = 0.98, which is orders of magnitude below what would be expected to characterize the flow as turbulent.

Foamed cement is a non-Newtonian fluid, often described as obeying a Hershel-Buckley relationship (Ahmed et al., 2009) where the shear stress (τ) within the fluid is described by a yield stress (τ_y), consistency and flow behavior indices (k and n), shear rate ($\dot{\gamma}$) that the fluid is experiencing. Madlener et al. (2009) included an apparent viscosity term (η_o) to describe the viscosity of Hershel-Buckley fluids at high shear rates as well. Foamed cement is thixotropic (viscosity goes down with increasing shear stress) so the η_o term is often very small.

$$\tau = \tau_y + k\dot{\gamma}^n + \eta_o . \tag{2}$$

When examining Hershel-Buckley fluids the Reynold's number in Equation 1 may not be appropriate because μ is not a constant. Madlener at al. (2009) developed the following relationship to describe the transition of laminar to turbulent flow of a Hershel-Buckley fluid,

$$\mathrm{Re}_{HB} = \left(\rho U^{2-n} L^n\right) \Big/ \left(\frac{\tau_y}{8}\left(\frac{L}{U}\right)^n + K\left(\frac{3m+1}{4m}\right)^n 8^{n-1} + \eta_o \frac{3m+1}{4m}\left(\frac{D}{U}\right)^{n-1}\right).$$

where

$$m = \frac{nK\left({}^{8U}/_{L}\right)^n + \eta_o\left({}^{8U}/_{L}\right)}{\tau_y + K\left({}^{8U}/_{L}\right)^n + \eta_o\left({}^{8U}/_{L}\right)}. \tag{3}$$

Examining Re_{HB} for the range of τ_y, n, and K presented in Ahmed et al. (2009) for 30% foamed cement, assuming $\eta_o \approx 0.3$ Pa*s from their highest shear rate tests, and using the geometric and velocity values previously presented Re_{HB} is approximately 0.1.

The flow through the transitional hammer union and bull plug was faster than the flow through the primary CP vessel chamber, but not the orders of magnitude increase that would be expected to cause turbulent flow. Since the initial collection described in this report, additional pressurized foamed cement collections using similar large scale industrial equipment have been performed with reduced U and foamed cement quality, and qualitatively the heterogeneous structure of the foamed cement voids is similar. This unpublished work will be presented in future reports, following more detailed analysis. The estimates of different fluid and flow properties, along with unpublished test results, indicate that turbulent flow within the vessels in unlikely.

At this time, several hypotheses as to what is causing the low density void distributions throughout the CP vessels are being examined. A choking mechanism as the foamed cement moves into the CP vessel may be inducing unique void formation, so different geometries are being examined with the FCG. The viscosity of the actual foamed cement may be widely different than described in previous works, so in-house measurements of pressurized fluid properties are planned. Pressure cycling of the cement as it is being pumped by upstream equipment may be influencing the structure, so cement created in the lab will be analyzed under varying pressure oscillations. Another potential contributing factor is the difference in method of inert gas introduction to the cement system.

This initial report has provided a unique view of a ubiquitous, yet unexamined, wellbore material, but a full grasp of the mechanisms that will enable the placement of a homogenous foamed cement in deep wellbores will require further research.

5. CONCLUSIONS

It appears that foamed cement BSD in the field-generated cements are strongly influenced by flow. The scans show a non-homogenous mixture of the slurry. The connected and localized nature of low and high porosity zones suggest that they were influenced by flow through the sample vessels. The larger bubbles may be indicative of the coarsening or clustering of smaller bubbles. These larger bubbles appear to be concentrated along the streak lines indicating the fluid motion within the sample vessels and may be comparable to flow in the annulus of a wellbore. Work is continuing to isolate flow, bubble distribution, and other relevant properties that can be engineered into safer and more efficient placement of foamed cement downhole.

The results illustrate that CT data can be effectively used to evaluate cements at in-situ pressure conditions. The medical CT images provided quick and moderate resolution data that can be used to evaluate the bulk density profile of an entire sample. Medical CT data also gives a macroscopic view of the flow dynamics within the vessel, which assists flow models on matching real world samples. Medical CT data was also used to evaluate which sections of the samples needed more detailed analysis; this enabled the researchers to focus their efforts on those foamed cement characteristics that have not been previously reported.

The industrial CT data gave researchers the ability to characterize the cements through multiple avenues. The observed patterns indicate a high level of complexity of in situ foamed cement behaviour. The structures seen in the full scans of the cores appear similar to particle clustering in turbulent flows. However, the Reynolds number of the cement flow in the vessel ($Re < 1$) was far below the minimum threshold for characterizing the flow as turbulent. The variations in cement structure within the pressurized foamed cement samples all appear to indicate a strong relationship between the flow of the cement and the final porosity and properties of the in-place hardened cement. Work is continuing to isolate flow, distribution, and other relevant properties that can be engineered into safer and more efficient placement of foamed cement downhole.

6. REFERENCES

Ahmed, R. M.; Takach, N. E.; Khan, U. M.; Taoutaou, S.; James, S.; Saasen, A.; Godøy, R. Rheology of foamed cement. *Cement and Concrete Research* **2009,** *39*, 353–361.

API 2004. API Recommended Practice 10B-4. Recommended Practice on Preparation and Testing of Foamed Cement Slurries at Atmospheric Pressure, 1st ed., American Petroleum Institute: Washington, DC.

API 2010. API Standard 65-2. Isolating Potential Flow Zones During Well Construction, 2nd ed., American Petroleum Institute: Washington, DC.

Benge, G.; Poole, D. *Use of foamed cement in deep water Angola*; SPE/IADC 91662; 2005.

Benge, O. G.; McDermott, J. R.; Langlinais, J. C.; Griffith, J. E. Foamed cement job successful in deep HTHP offshore well. *Oil and Gas Journal* **1996,** *94*, 58–63.

de Rozieres, J.; Ferriere, R. Foamed-cement characterization under downhole conditions and its impact on job design. *SPE Production Engineering* **1991,** *6*, 297–304.

Deeg W.; Griffith, J.; Crook, R.; Benge, G. How Foamed Cement Advantages Extend to Hydraulic Fracturing Operations. *World Oil* **1999,** *220*, 51–53.

Frisch, G. J.; Graham, W. L.; Griffith, J. Assessment of foamed-cement slurries using conventional cement evaluation logs and improved interpretation methods. SPE Rocky Mountain Regional Meeting, Gillette, WY, May 15–18, 1999; SPE 55649.

Griffith, J. E; Lende, G.; Ravi, K.; Saasen, A.; Nødland, N. E.; Jordal, O. H. Foam cement engineering and implementation for cement sheath integrity at high temperature and high pressure. IADC/SPE Drilling Conference, Dallas, TX, March 2–4, 2004; SPE 87194.

Harlan, T. D.; Foreman, J. M.; Reed, S. D.; Griffith, J. E. Foamed cement selection for horizontal liners proves effective for zonal isolation—case history. SPE Rocky Mountain Petroleum Technology Conference, Keystone, CO, May 21–23, 2001; SPE 71055.

Harms, W. M.; Febus, J. S. Cementing of fragile-formation wells with foamed cement slurries. *Journal of Petroleum Technology* **1985,** *37*, 1049–1057.

Iverson, B.; Darbe, R.; McMechan, D. Evaluation of Mechanical Properties of Cements; 2008; ARMA 08-293.

Judge, R. A.; Benge, G. Advances in metering and control technology improves design and execution of foamed cement jobs. IADC/SPE Asia Pacific Drilling Technology, Jakarta, Indonesia, Sept 7–9, 1998; IADC/SPE 47831.

Keller, A. A. High resolution cat imaging of fractures in consolidated materials. *International Journal of Rock Mechanics and Mining Sciences* **1997,** *34*, 155.e1–155.e16.

Kopp, K.; Reed, S.; Foreman, J.; Carty, B.; Griffith, J. Foamed cement vs. conventional cement for zonal isolation – case histories. Computed Tomography and Statistical Analysis of Bubble Size Distributions in Atmospheric-Generated Foamed Cement. SPE Annual Technical Conference and Exhibition, Dallas, TX, Oct 1–4, 2000; SPE 62895.

Kutchko, B.; Crandall, D.; Gill, M.; McIntyre, D.; Spaulding, R.; Strazisar, B.; Rosenbaum, E.; Haljasmaa, I.; Benge, G.; Cunningham, E.; DeBruijn, G.; Gardner, C. *Computed Tomography and Statistical Analysis of Bubble Size Distributions in Atmospheric-*

Generated Foamed Cement; NETL-TRS-2-2013; EPAct Technical Report Series; U.S. Department of Energy, National Energy Technology Laboratory: Morgantown, WV, 2013; p 28.

Kutchko, B.; Moore, J.; Crandall, D.; Gill, M.; McIntyre, D.; Spaulding, R.; Strazisar, B.; Rosenbaum, E.; Haljasmaa, I.; Benge, G.; Cunningham, E.; DeBruijn, G.; Shine, J.; Gardner, C. *Addendum 1 to Computed Tomography and Statistical Analysis of Bubble Size Distributions in Atmospheric-Generated Foamed Cement*; NETL-TRS-2-2014; EPAct Technical Report Series; U.S. Department of Energy, National Energy Technology Laboratory: Morgantown, WV, 2014; p 20.

Kutchko, B.; Pike, W.; Lang, K.; Strazisar, B.; Rose, K. *An assessment of research needs related to improving primary cement isolation of formations in deep offshore wells*; NETL-TRS-3-2012; EPAct Technical Report Series; U.S. Department of Energy, National Energy Technology Laboratory: Morgantown, WV, 2012; p 20.

Madlener, K.; Frey, B.; Ciezki, H. K. Generalized Reynolds Number for Non-Newtonian Fluids. *Progress in Propulsion Physics* **2009,** *1*, 237–250.

Moore, S.; Miller, M.; Faul, R. Foam cementing applications of a deepwater subsalt well—case history. IADC/SPE Drilling Conference, New Orleans, LA, Feb 23–25, 2000; IADC/SPE 59170.

Nasr, H.; Ahmadi, G.; McLaughlin, J. B. A DNS Study of Effects of Particle-Particle Collisions and Two-Way Coupling on Particle Deposition and Phasic Fluctuations. *Journal of Fluid Mechanics* **2009,** *640*, 507–536.

Nelson, E. B., Ed. *Well Cementing*; Schlumberger Educational Services: Sugar Land, TX, 2006.

Rae, P.; Lullo, G. D. Lightweight cement formulations for deep water cementing: Fact and fiction. SPE Annual Technical Conference and Exhibition, Houston, TX, Sept 26–29, 2004; SPE 91002.

Rasband, W. S.; ImageJ. U.S. National Institutes of Health: Bethesda, MD, 1997–2013. http://imagej.nih.gov/ij/ (accessed 2012).

Taiwo, O.; Ogbonna, J. Foam cementing design and application: A cure for low gradient associated problems in deepwater operations in the Gulf of Guinea. Nigeria Annual International Conference and Exhibition, Abuja, Nigeria, July 30–Aug 3, 2011; SPE 150767.

Thayer, R. D.; Ford, D. G.; Holekamp, S.; Pferdehirt, D. J. Real-time quality control of foamed cement jobs: A case study. SPE Annual Technical Conference and Exhibition, Houston, TX, Oct 3–6, 1993; SPE 26575.

Thévenaz, P.; Ruttimann, U. E.; Unser, M. A pyramid approach to subpixel registration based on intensity. *IEEE Transactions on Image Processing* **1998,** *7*, 27–41.

White, F. M. Fluid Mechanics, 4th ed.; McGraw-Hill, 1999.

White, J.; Moore, S.; Miller, M.; Faul, R. Foaming cement as a deterrent to compaction damage in deepwater production. IADC/SPE Drilling Conference, New Orleans, LA, Feb 23–25, 2000; IADC/SPE 59136.

This page intentionally left blank.

Jared Ciferno
Director
Strategic Center for Natural Gas and Oil
National Energy Technology Laboratory
U.S. Department of Energy

Elena Melchert
Program Manager
Oil and Gas Production
Office of Fossil Energy
U.S. Department of Energy

Maria Vargas
Deputy Director
Strategic Center for Natural Gas and Oil
National Energy Technology Laboratory
U.S. Department of Energy

Cynthia Powell
Director
Office of Research and Development
National Energy Technology Laboratory
U.S. Department of Energy

Roy Long
Technology Manager
Strategic Center for Natural Gas and Oil
National Energy Technology Laboratory
U.S. Department of Energy

Kevin Donovan
RES Program Manager
URS Corporation